International Journal for Numerical Methods in Engineering

WILEY

RESEARCH ARTICLE OPEN ACCESS

Stabilized Mixed Formulations for Incompressible Finite Strain Electromechanics Including Stress Accurate Analysis

Inocencio Castañar[1,2] | Jesús Martínez-Frutos[2] | Rogelio Ortigosa[2] | Ramon Codina[3,4]

[1]Department of Mechanical Engineering, Universitat Politècnica de Catalunya-BarcelonaTech (UPC), Escola d'Enginyeria de Barcelona Est, Barcelona, Catalunya, Spain | [2]Multiphysic Simulation & Optimization Lab, Department of Structures and Construction, Technical University of Cartagena, Cartagena, Murcia, Spain | [3]Department of Civil and Environmental Engineering, Universitat Politècnica de Catalunya–BarcelonaTech (UPC), Barcelona, Catalunya, Spain | [4]Centre Internacional de Mètodes Numèrics en Enginyeria (CIMNE), Barcelona, Spain

Correspondence: Inocencio Castañar (inocencio.castanar@upc.edu)

Received: 9 January 2025 | **Revised:** 30 June 2025 | **Accepted:** 16 July 2025

Funding: This work was supported by the MICIU/AEI/10.13039/501100011033, Spain grant PID2022-141957OA-C22, and by "ERDF A way of making Europe." Autonomous Community of the Region of Murcia, Spain, through the programme for the development of scientific and technical research by competitive groups (21996/PI/22), included in the Regional Programme for the Promotion of Scientific and Technical Research of Fundación Séneca – Agencia de Ciencia y Tecnología de la Región de Murcia. Institució Catalana de Recerca i Estudis Avançats (ICREA) Acadèmia Research Program of the Generalitat de Catalunya.

Keywords: electromechanics | incompressible hyperelasticity | mixed formulations | orthogonal subgrid scales | stabilization methods

ABSTRACT

In this study, we introduce a novel methodology for finite strain electromechanics that effectively addresses the incompressible limit. The primary innovation of this work is the first-time application of robust and accurate stabilized mixed formulations, previously developed by the authors for hyperelasticity, within the realm of electromechanics. These formulations incorporate the pressure field as an unknown variable, thereby facilitating the automatic attainment of the incompressible limit. Additionally, we consider the mechanical deviatoric stress tensor as a primary unknown, allowing for the design of finite element technology capable of managing incompressible behavior while ensuring high accuracy in the stress field and avoiding shear locking of thin solids. To enable the use of equal-order interpolations, we employ the orthogonal subgrid scale method for stabilization. Furthermore, the electromechanical problem is approached through a block-iterative staggered method. We present a series of numerical examples to assess the robustness and applicability of these formulations in solving complex finite strain electromechanics problems.

1 | Introduction

Electroactive Polymers (EAPs) have emerged as a versatile class of smart materials due to their ability to undergo large deformations in response to electrical stimuli [1, 2]. These materials have found applications in a wide range of fields, including soft robotics, sensors, actuators, and artificial muscles [3, 4]. EAPs are broadly categorized into two types: Ionic and electronic. Ionic EAPs, such as ionic polymer-metal composites (IPMCs), rely on ion transport mechanisms and generally require moisture to function. Electronic EAPs, on the other hand, are driven by electric field-induced forces and include materials like piezoelectric polymers and dielectric elastomers (DEs). Among these, DEs have gained particular attention due to their high energy density, large actuation strains, and fast response times [5].

DEs are a subset of electronic EAPs that function as soft capacitors. When a voltage is applied across their compliant electrodes, the resulting electrostatic forces cause the elastomer to deform [3, 5]. This actuation mechanism makes DEs highly promising for applications requiring large, reversible deformations. Additionally, DEs exhibit excellent scalability, lightweight properties, and high flexibility, making them suitable for soft actuators and energy harvesting devices [6–8].

The study of DEs inherently involves complex, nonlinear solid mechanics due to the large deformations and highly coupled electro-mechanical behavior they exhibit. When subjected to electric fields, DEs undergo significant strains, often exceeding 100%, which places them well outside the linear elasticity regime [9]. As a result, classical linear mechanics approaches are insufficient to capture their full behavior. Nonlinear solid mechanics is essential for accurately modeling the material's response to both mechanical and electrical stimuli [10–12]. Many DEs exhibit behavior that is nearly or fully incompressible, meaning their volume remains constant or nearly constant during deformation. This incompressibility presents a significant challenge when modeling their mechanical behavior, as traditional material models may fail to capture this constraint accurately. The incompressibility of DEs arises from their rubber-like nature, which causes large shape changes without corresponding volume changes under applied stresses or electric fields. To account for this, specialized constitutive models that incorporate incompressibility are essential in the characterization of DEs. Neglecting this aspect can lead to inaccurate predictions of material performance, such as incorrect strain distributions or stress concentrations, especially under large deformations [13–17].

DEs are commonly modeled using the framework of continuum mechanics to capture their coupled electro-mechanical behavior under large deformations [18–26]. The reversible constitutive model of these materials is encapsulated within the free energy density, in terms of invariants of the deformation gradient tensor and the material electric field [27–29]. Complementary to this potential, which exhibits a saddle point nature, is the internal energy density, which depends upon the deformation gradient tensor and the electric displacement field. Building upon this foundation, researchers in [30–32] introduced an extension of the concept of polyconvexity, originally from the field of hyperelasticity [33–40], into this coupled electromechanical scenario. This novel definition of polyconvexity played a pivotal role in establishing the existence of minimizers in this context for the first time [41], serving as a sufficient condition for the extension of the rank-one convexity criterion within electromechanics.

For the numerical simulation of DEs, the finite element method (FEM) is widely used due to its flexibility in handling complex geometries and boundary conditions. In this approach, the DE is discretized into finite elements (FEs), and the governing equations are derived from the principles of nonlinear elasticity and electrostatics. Special attention is given to the near-incompressibility of DEs, which requires tailored FE formulations, such as mixed methods introducing the pressure as a variable, either using appropriate interpolations for it or stabilization techniques, to avoid locking phenomena. This combination of continuum-based material models and FE analysis allows for accurate prediction of the electro-mechanical response of DEs, providing valuable insights for optimizing their performance in various applications.

Previous studies have adopted mixed formulations that incorporate not only primary variables, such as displacements and electric potential, but also derived variables, like strains and electric fields, into the set of unknowns [42, 43]. For example, Ortigosa et al. [44] introduced an advanced mixed formulation in which fields central to polyconvexity in electro-mechanics—namely, the deformation gradient tensor ($\boldsymbol{F}$), its cofactor, its determinant, the electric displacement field $\boldsymbol{d}_0$, and an additional coupled field $\boldsymbol{F} \cdot \boldsymbol{d}_0$—are included alongside their respective work conjugates as unknowns (see also [45] and [46] in the purely mechanical context). Here, the work conjugates act as Lagrange multipliers, weakly enforcing the necessary compatibility conditions. Notably, this formulation addresses the fully incompressible case and employs field discretizations that satisfy the inf-sup condition [47] without requiring additional stabilization.

In the context of continuum mechanics, low-order displacement-based FEs exhibit poor performance in nearly and fully incompressible conditions [48]. Issues such as volumetric and shear locking, pressure oscillations, and sub-optimal results in bending-dominated cases are common [49]. Mixed formulations are a well-established approach frequently used to address these numerical instabilities. Under the assumption of infinitesimal strain, a mixed formulation based on displacements and pressure [15, 50–52] is essential for dealing with the incompressible limit. Various stabilization techniques, particularly within the Variational Multi-Scale (VMS) framework [53], enable the use of equal-order, piecewise linear interpolations for all primary fields. Given the strong performance of mixed methods, [54] introduced a three-field displacement/pressure/deviatoric stress formulation, which proved highly effective for incompressible problems requiring precise stress and strain predictions (see also [13]). These FE technologies have shown enhanced accuracy in stress computation, successfully capturing stress concentrations and strain localizations, while ensuring stress convergence as the mesh is refined [55–57]. In previous studies, in the context of finite strain, the authors have developed stabilized mixed formulations for hyperelastic materials. First, a stabilized mixed displacement/pressure approach was introduced in [58] for nearly and fully incompressible hyperelastic material models, where stabilization was achieved using the VMS framework. More recently, in [59], a mixed three-field formulation that incorporates displacement, pressure, and deviatoric stress, utilizing equal-order interpolations for all primary variables, is proposed. Note that all the formulations described do not require inf-sup conditions between interpolating spaces to be satisfied. This is achieved by introducing some sort of stabilization mechanism, one of which is employed in this work. The literature about mixed formulations employing different interpolating spaces to achieve inf-sup stability is vast and will not be reviewed here.

The present manuscript extends these concepts to propose a novel way to solve the nonlinear electromechanics problem. Through the well-known deviatoric/volumetric decomposition of the mechanical part of the strain energy function, we complement the conservation of linear momentum equation with the constitutive equation of the pressure. This equation is written so as to allow imposing the incompressibility constraint on electromechanical materials in a natural way. Two different FE formulations are presented in this work. First, the $\boldsymbol{u}p\varphi$ formulation, which considers displacements, pressure, and electric potential field as primary unknowns. The resulting method is very simple, and only the addition of a scalar field as an extra primary variable is required with respect to the irreducible one. Next, a step forward is made to introduce the mixed $\boldsymbol{u}p\boldsymbol{S}'\varphi$ formulation where deviatoric stresses are also considered as primary variables of the problem. The only requirement is the introduction of the constitutive law for deviatoric stresses in the system of equations to be solved. This technology is expected to enhance stress accuracy as well as to increase the ability to capture stress concentrations with the guarantee of stress convergence upon mesh refinement. To consider equal-order interpolations for all master fields, the resulting formulations will be stabilized by means of the VMS-Orthogonal SubGrid Scale (OSGS) method, which is a stabilization technique well known for its low dissipative and highly accurate performance [60]. The objective of this work is to develop block-iterative schemes to solve the electromechanical problem, where coupling can be observed in both directions [61].

This work is organized as follows. In Section 2, some preliminaries are introduced to provide some key concepts, methodologies, and background knowledge. Next, in Section 3, the nonlinear continuum electromechanics equations are summarized. Section 4 presents two stabilized mixed formulations which are able to tackle the incompressible limit for electromechanics in finite strain theory. Afterwards, Section 5 briefly describes the concept of block-iterative schemes for coupled problems and their application to the electromechanical problem under investigation. In Section 6, several benchmarks and numerical examples are tested to assess the present formulation and to validate its performance. To end up, in Section 7, some conclusions of the proposed formulation are drawn.

2 | Preliminaries

This section provides a foundational introduction to the key concepts, theories, methodologies, and background knowledge necessary for understanding the main content of the coupled problem presented in this work.

2.1 | Notation

Throughout this paper, $\boldsymbol{A} : \boldsymbol{B} = A_{ij}B_{ij}$, $\forall \boldsymbol{A}, \boldsymbol{B} \in \mathbb{R}^{3\times3}$, and the use of repeated indices implies summation. The tensor product is denoted by $\otimes$ and the second-order identity tensor by $\boldsymbol{I}$. The tensor cross product operation $\times$ between two arbitrary second-order tensors $\boldsymbol{A}$ and $\boldsymbol{B}$ entails $[\boldsymbol{A} \times \boldsymbol{B}]_{il} = \mathcal{E}_{ijk}\mathcal{E}_{lmn}A_{jm}B_{kn}$. Furthermore, $\boldsymbol{\mathcal{E}}$ represents the third-order alternating tensor. Regarding the product between matrices and vectors, or matrices and matrices, $[\boldsymbol{A} \cdot \boldsymbol{B}]_{ik} = A_{ij}B_{jk}$,

$\forall \boldsymbol{A}, \boldsymbol{B} \in \mathbb{R}^{3\times3}$, or $[\boldsymbol{A}\cdot\boldsymbol{B}]_i = A_{ij}B_j, \forall \boldsymbol{A} \in \mathbb{R}^{3\times3}, \boldsymbol{B} \in \mathbb{R}^3$. When the product involves a scalar, the symbol will be omitted to improve the readability of the text.

2.2 | Weak Formulation

Let us introduce some notation for deriving the weak formulation of the formulations we need to develop. As usual, the space of square integrable functions in a domain υ is denoted by $L^2(\upsilon)$, whereas the space of functions whose first derivative is square integrable is denoted by $H^1(\upsilon)$. We shall use the symbol $\langle\cdot,\cdot\rangle_\upsilon$ to refer to the integral of the product of two functions in a domain υ, not necessarily in $L^2(\upsilon)$. The subscript is omitted when $\upsilon = V$, being V the domain of study.

2.3 | Load Increments to Solve Nonlinear Equations

In the case of large deformations, it is customary to solve the nonlinear equilibrium equations in an incremental manner for steps $n = 0, \dots, N$, being N the maximum number of load increments. The external forces are applied incrementally, their magnitude being controlled by an incremental factor λ^n at a given load increment n, such that $\lambda^n = n/N$. For simplicity, we will consider constant load increments, although the extension to variable load increments would be straightforward.

2.4 | Spatial Discretization

For all formulations, the standard FE approximation is considered as follows. Let $\mathcal{P}_h$ denote a FE partition of the domain of study V. The diameter of an element domain $K \in \mathcal{P}_h$ is denoted by h_K and the diameter of the FE partition by $h = \max\{h_K | K \in \mathcal{P}_h\}$. We can now construct conforming FE spaces $\mathcal{V}_h \subset \mathcal{V}$ being $\mathcal{V}$ any proper functional space where an unknown solution is well-defined, as well as the corresponding subspace $\mathcal{V}_{h,0} \subset \mathcal{V}_0$, $\mathcal{V}_0$ being made with functions that vanish on the Dirichlet boundary.

2.5 | The VMS Framework

To circumvent the complexities associated with mixed interpolations that satisfy the necessary inf-sup conditions [62, 63], we prefer utilizing stabilized FE methods that allow for uniform interpolations across all variables. The formulations introduced in this study are grounded in the VMS framework [53, 64]; thus, we provide a summary of the formulation here, highlighting the aspects that are pertinent to the problem under consideration.

Let us consider a nonlinear stationary problem of the form $\mathscr{A}(\boldsymbol{U}) = \lambda f$, where $\mathscr{A}(\boldsymbol{U})$ is a nonlinear operator and λ is the load factor. Suppose that this equation is solved by an iterative scheme, so that given a guess for the solution, still denoted $\boldsymbol{U}$, the correction $\boldsymbol{\delta U}$ is computed from the equation

$$\mathscr{L}(\boldsymbol{U};\boldsymbol{\delta U}) = \lambda f - \mathscr{A}(\boldsymbol{U}),$$

where $\mathscr{L}(\boldsymbol{U};\boldsymbol{\delta U})$ is linear in $\boldsymbol{\delta U}$. The weak form of the problem results from the integration-by-parts formula

$$B(\boldsymbol{U};\boldsymbol{V},\boldsymbol{\delta U}) := \langle \boldsymbol{V}, \mathscr{L}(\boldsymbol{U};\boldsymbol{\delta U})\rangle = \langle \boldsymbol{V}, \lambda f - \mathscr{A}(\boldsymbol{U})\rangle := L(\boldsymbol{V},\boldsymbol{U}) \quad \forall \boldsymbol{V} \in \mathcal{V}. \tag{1}$$

We have considered homogeneous boundary conditions to simplify the explanation, so that the spaces for the unknowns and the test functions are the same. In the second term, the divergence of the appropriate fluxes is considered integrated by parts.

Once the FE approximation is set, the Galerkin approximation to Equation (1) consists of finding $\boldsymbol{\delta U}_h \in \mathcal{V}_h$ such that

$$B\big(\boldsymbol{U}_h;\boldsymbol{V}_h,\boldsymbol{\delta U}_h\big) = L\big(\boldsymbol{V}_h,\boldsymbol{U}_h\big) \quad \forall \boldsymbol{V}_h \in \mathcal{V}_h.$$

This problem is well posed, that is, it has a unique solution bounded in the norm of $\mathcal{V}$ independently of h, if the following condition holds (see, e.g., [63]):

$$\inf_{\delta \boldsymbol{U}_h \in \mathcal{V}_h} \sup_{\boldsymbol{V}_h \in \mathcal{V}_h} \frac{B(\boldsymbol{U}_h; \boldsymbol{V}_h, \delta \boldsymbol{U}_h)}{\|\delta \boldsymbol{U}_h\|_{\mathcal{V}} \|\boldsymbol{V}_h\|_{\mathcal{V}}} \geq K_B > 0, \tag{2}$$

for a certain constant K_B. For all the problems presented in this work, $\mathcal{V}_h$ is obtained from the Cartesian product of two or three spaces, and the previous inf-sup condition poses stringent compatibility conditions on the choice of these FE spaces. Note that the continuous counterpart of Equation (2), replacing $\mathcal{V}_h$ by $\mathcal{V}$, is known to hold for all problems considered. This fact motivates the need to introduce stabilized FE methods. The key idea of the VMS approach is to split the space $\mathcal{V}$ as $\mathcal{V} = \mathcal{V}_h \oplus \tilde{\mathcal{V}}$, where $\tilde{\mathcal{V}}$ is any space to complete $\mathcal{V}_h$ in $\mathcal{V}$. The elements of this space are denoted by $\tilde{\boldsymbol{U}}$ and they are called subgrid scales (SGSs).

This splitting will have the associated splitting of the unknowns and tests functions $\boldsymbol{U} = \boldsymbol{U}_h + \tilde{\boldsymbol{U}}$ and $\boldsymbol{V} = \boldsymbol{V}_h + \tilde{\boldsymbol{V}}$, with $\boldsymbol{U}_h, \boldsymbol{V}_h \in \mathcal{V}_h$ and $\tilde{\boldsymbol{U}}, \tilde{\boldsymbol{V}} \in \tilde{\mathcal{V}}$. Because of the linearity of the problem (1) considered so far, we may write the continuous problem as: Find $\delta \boldsymbol{U}_h \in \mathcal{V}_h$ and $\tilde{\boldsymbol{U}} \in \tilde{\mathcal{V}}$ such that

$$B(\boldsymbol{U}_h; \boldsymbol{V}_h, \delta \boldsymbol{U}_h) + B(\boldsymbol{U}_h; \boldsymbol{V}_h, \tilde{\boldsymbol{U}}) = L(\boldsymbol{V}_h, \boldsymbol{U}_h) \quad \forall \boldsymbol{V}_h \in \mathcal{V}_h, \tag{3a}$$

$$B(\boldsymbol{U}_h; \tilde{\boldsymbol{V}}, \delta \boldsymbol{U}_h) + B(\boldsymbol{U}_h; \tilde{\boldsymbol{V}}, \tilde{\boldsymbol{U}}) = L(\tilde{\boldsymbol{V}}, \boldsymbol{U}_h) \quad \forall \tilde{\boldsymbol{V}} \in \tilde{\mathcal{V}}. \tag{3b}$$

To avoid approximating derivatives of $\tilde{\boldsymbol{U}}$, and require only the unknown $\tilde{\boldsymbol{U}}$ itself, making use of the additivity of the integral, we may write Equation (3a) as

$$B(\boldsymbol{U}_h; \boldsymbol{V}_h, \delta \boldsymbol{U}_h) + \sum_K \langle \mathscr{L}^*(\boldsymbol{U}_h; \boldsymbol{V}_h), \tilde{\boldsymbol{U}} \rangle_K = L(\boldsymbol{V}_h, \boldsymbol{U}_h) \quad \forall \boldsymbol{V}_h \in \mathcal{V}_h, \tag{4}$$

where $\mathscr{L}^*(\boldsymbol{U}; \boldsymbol{V})$ is linear in $\boldsymbol{V}$ and it is defined as the adjoint operator of $\mathscr{L}(\boldsymbol{U}; \delta \boldsymbol{U})$. Inter-element boundary terms have been discarded, but they could be introduced following the ideas in [65]. Equation (4) will be our FE problem once $\tilde{\boldsymbol{U}}$ is approximated in terms of $\boldsymbol{U}_h$. The description of how to attempt this will be omitted, and only the final result will be stated. In any case, this approximation must be obtained from Equation (3b), which may be written as

$$\begin{aligned} B(\boldsymbol{U}_h; \tilde{\boldsymbol{V}}, \tilde{\boldsymbol{U}}) &= \sum_K \langle \tilde{\boldsymbol{V}}, \mathscr{L}(\boldsymbol{U}_h; \tilde{\boldsymbol{U}}) \rangle_K = L(\tilde{\boldsymbol{V}}, \boldsymbol{U}_h) - B(\boldsymbol{U}_h; \tilde{\boldsymbol{V}}, \delta \boldsymbol{U}_h) \\ &= \sum_K \langle \tilde{\boldsymbol{V}}, \lambda f - \mathscr{A}(\boldsymbol{U}_h) \rangle_K - \sum_K \langle \tilde{\boldsymbol{V}}, \mathscr{L}(\boldsymbol{U}_h; \delta \boldsymbol{U}_h) \rangle_K \quad \forall \tilde{\boldsymbol{V}} \in \tilde{\mathcal{V}}, \end{aligned} \tag{5}$$

where we have assumed the SGSs to behave as bubble functions, which means that they vanish across inter-element boundaries. As explained in [65], this assumption can be relaxed, and the SGSs can be approximated on these boundaries. We shall come back to this point later.

All VMS-type methods consist in approximating $\tilde{\boldsymbol{U}}$ from Equation (5). This is the problem that requires approximation, with several options detailed in [64]. Our preferred approach applies Fourier analysis to the problem. This approximate Fourier analysis of the SGS problem was initially proposed in [66] and later extended in [67]. The key heuristic assumption here is that the SGS is highly fluctuating, thus being dominated by high wave numbers. Regarding the approximation of the SGSs in the interior of the element domains, from Equation (5) it turns out that we may approximate it within each element K as (see [64]):

$$\tilde{\boldsymbol{U}}|_K = \boldsymbol{\tau}_K \tilde{\Pi} [\lambda f - \mathscr{A}(\boldsymbol{U}_h) - \mathscr{L}(\boldsymbol{U}_h; \delta \boldsymbol{U}_h)]|_K,$$

where $\tilde{\Pi}$ is the $L^2(V)$ projection onto the space of SGSs, which still needs to be chosen, and $\boldsymbol{\tau}_K$ is a matrix of stabilization parameters that tries to approximate (in an integral sense) operator $\mathscr{L}^{-1}$. We shall come back later on to its expression for the problems we are considering. Regarding the space of SGSs and the associated projection $\tilde{\Pi}$, we consider taking $\tilde{\mathcal{V}} = \mathcal{V}_h^{\perp}$, that is, the $L^2(V)$-orthogonal to the FE space. This leads to the OSGS approach [66], case in which $\tilde{\Pi} = \mathtt{I} - \Pi_h$, where Π_h is the $L^2(V)$-projection onto the FE space and $\mathtt{I}$ the identity operator. The stabilized problem to be solved is: Find $\delta \boldsymbol{U}_h \in \mathcal{V}_h$ such that

$$B(\boldsymbol{U}_h; \boldsymbol{V}_h, \delta \boldsymbol{U}_h) + \sum_K \langle \mathscr{L}^*(\boldsymbol{U}_h; \boldsymbol{V}_h), \boldsymbol{\tau}_K \tilde{\Pi} [\lambda f - \mathscr{A}(\boldsymbol{U}_h) - \mathscr{L}(\boldsymbol{U}_h; \delta \boldsymbol{U}_h)] \rangle_K = L(\boldsymbol{V}_h, \boldsymbol{U}_h) \quad \forall \boldsymbol{V}_h \in \mathcal{V}_h. \tag{6}$$

A key property of the OSGS stabilization is that, thanks to the projection orthogonal to the FE space, we keep the consistency of the formulation in a weak sense in spite of including just the minimum number of terms to stabilize the solution. This property allows us to propose a term-by-term type stabilization technique called Split-OSGS (S-OSGS). The S-OSGS method is not just a simplification of the OSGS one. For smooth solutions, both have an optimal convergence rate in mesh size. However, in problems where the solution has strong gradients, we have found the S-OSGS more robust, similarly to what is explained in [55]. This method allows us to select only the terms that contribute to the stability of the problem. Later, for each formulation developed in this work, the operators and stabilization matrix used will be determined. It will be seen that in our case, rather than a term-by-term stabilization, we simply need to include one term from the linearization of the momentum equation and another one from the linearization of the continuity equation. To emphasize that the operators involved in Equation (6) do not contain all the terms of the original problem, we will characterize them by the symbol $\hat{\cdot}$ in the following.

3 | Nonlinear Continuum Electromechanics

This section outlines the system of coupled partial differential equations within the framework of reversible electromechanics, where dissipative effects are neglected. It also presents the constitutive relations that characterize the material's response.

3.1 | Kinematics: Motion and Deformation

Let us consider the motion of an electro-active body which in its initial or material configuration is defined by an open, bounded, and polyhedral domain V of $\mathbb{R}^d$, where $d \in \{2, 3\}$ is the number of space dimensions. The boundary of the reference configuration is ∂V with outward unit normal $\boldsymbol{N}$. After the motion, the body occupies a spatial configuration defined by a domain v with boundary ∂v. The motion is described by a pseudo-time t dependent mapping field $\boldsymbol{\phi}$ which links a material particle from $\boldsymbol{X} \in V$ to the spatial configuration $\boldsymbol{x} \in v$ according to

$$\boldsymbol{\phi} : V \to v(t), \quad \boldsymbol{x} = \boldsymbol{\phi}(\boldsymbol{X}, t), \quad \forall \boldsymbol{X} \in V, \quad t \geq 0.$$

The displacement field is defined as $\boldsymbol{u} = \boldsymbol{x} - \boldsymbol{X} = \boldsymbol{\phi}(\boldsymbol{X}, t) - \boldsymbol{X}$ and Dirichlet boundary conditions are imposed as $\boldsymbol{u} = \boldsymbol{u}_{\mathrm{D}}$ on the boundary $\partial V_{\mathrm{u}} \subset \partial V$. Associated with the mapping $\boldsymbol{\phi}$, it is possible to define the deformation gradient tensor or fiber-map $\boldsymbol{F}$, which is defined as the material gradient operator $\boldsymbol{\nabla}_0(\cdot)$ of the spatial configuration, namely

$$\boldsymbol{F} = \boldsymbol{\nabla}_0 \boldsymbol{x} = \frac{\partial \boldsymbol{\phi}(\boldsymbol{X}, t)}{\partial \boldsymbol{X}}.$$

In addition, $J = \det \boldsymbol{F} > 0$ represents the Jacobian or volume-map of the deformation. We can also define the right Cauchy-Green strain tensor, $\boldsymbol{C} = \boldsymbol{F}^{\mathrm{T}} \cdot \boldsymbol{F}$, as a symmetric kinematic measure.

3.2 | Solid Mechanics: Conservation of Linear and Angular Momentum

One of the fundamental equations governing nonlinear electromechanics is the global conservation of linear momentum. In the absence of inertial effects, this principle can be expressed as the integral translation equilibrium equation, namely

$$\int_{\partial V} \boldsymbol{t}_0 \, dA + \int_V \boldsymbol{f}_0 \, dV = \boldsymbol{0},$$

where $\boldsymbol{f}_0$ represents the body force per unit undeformed volume V and $\boldsymbol{t}_0$ the traction force per unit undeformed area, which is known at the Neumann boundary $\partial V_{\mathrm{t}} \subset \partial V$ such that $\partial V_{\mathrm{u}} \cup \partial V_{\mathrm{t}} = \partial V$ and $\partial V_{\mathrm{u}} \cap \partial V_{\mathrm{t}} = \emptyset$. The local form of the conservation of linear momentum and the associated boundary conditions can be written as

$$-\boldsymbol{\nabla}_0 \cdot \{\boldsymbol{F} \cdot \boldsymbol{S}\} = \boldsymbol{f}_0 \quad \text{in V}, \tag{7a}$$

$$\{\boldsymbol{F} \cdot \boldsymbol{S}\} \cdot \boldsymbol{N} = \boldsymbol{t}_0 \quad \text{on } \partial V_{\mathrm{t}}, \tag{7b}$$

$$\boldsymbol{u} = \boldsymbol{u}_{\mathrm{D}} \quad \text{on } \partial V_{\mathrm{u}}, \tag{7c}$$

where $\boldsymbol{S}$ represents the second Piola-Kirchhoff (PK2) stress tensor and $\boldsymbol{\nabla}_0 \cdot (\cdot)$ is the material divergence operator. Furthermore, conservation of angular momentum leads to the well-known symmetry tensor condition $\boldsymbol{S}^{\mathrm{T}} = \boldsymbol{S}$.

3.3 | Electrostatics: Gauss's and Faraday's Laws

In addition to the conservation of linear and angular momentum presented in Section 3.2, the dielectric elastomer represented by the continuum described in Section 3.1 is subjected in its material configuration V to an electric volume charge ρ_0^{e} per unit of undeformed volume and an electric surface charge ω_0^{e} per unit of undeformed area applied on $\partial V_\omega \subset \partial V$. The integral version of Gauss's law can be written in a Lagrangian format as

$$\int_{\partial V} \omega_0^{\mathrm{e}}\, dA + \int_V \rho_0^{\mathrm{e}}\, dV = 0.$$

The local form of Gauss's law and its associated boundary conditions can be written as

$$\begin{aligned} \boldsymbol{\nabla}_0 \cdot \boldsymbol{D}_0 &= \rho_0^{\mathrm{e}} \qquad \text{in } V, \\ \boldsymbol{D}_0 \cdot \boldsymbol{N} &= -\omega_0^{\mathrm{e}} \quad \text{on } \partial V_\omega, \end{aligned}$$

where $\boldsymbol{D}_0$ is the Lagrangian electric displacement field. Furthermore, in the absence of magnetic fields, the integral version of the static Faraday's law can be written in a Lagrangian format for a closed curve C embedded in $V \cup \partial V$ as

$$\oint_C \boldsymbol{E}_0 \cdot d\boldsymbol{X} = 0,$$

where $\boldsymbol{E}_0$ is the Lagrangian electric field. The local form of the static Faraday's law and the associated boundary conditions can be expressed as

$$\begin{aligned} \boldsymbol{E}_0 &= -\boldsymbol{\nabla}_0 \varphi \quad \text{in } V, \\ \varphi &= \varphi_{\mathrm{D}} \qquad \text{on } \partial V_\varphi, \end{aligned}$$

where φ is an electric potential field that can be introduced in the case of a contractible domain. Dirichlet boundary conditions for the electric potential field are imposed on $\partial V_\varphi \subset \partial V$, such that $\partial V_\varphi \cup \partial V_\omega = \partial V$ and $\partial V_\varphi \cap \partial V_\omega = \emptyset$.

3.4 | Constitutive Model: The Free Energy Density

Let us focus on reversible electro-elasticity, where thermal effects and electric polarization-induced hysteresis are neglected. In this case, the free energy density Ψ per unit of undeformed volume can be solely defined in terms of the deformation and the electric field, namely $\Psi = \Psi(\boldsymbol{F}, \boldsymbol{E}_0)$. The requirement for objectivity (i.e., invariance with respect to rotations in the material configuration) implies that Ψ must be independent of the rotational components of the deformation. This can be achieved by re-expressing the free energy density in terms of the right Cauchy-Green tensor $\boldsymbol{C}$, resulting in $\Psi = \Psi(\boldsymbol{C}, \boldsymbol{E}_0)$.

Typically, the free energy density $\Psi(\boldsymbol{C}, \boldsymbol{E}_0)$ is additively decomposed into a purely mechanical component, denoted as $\Psi_m(\boldsymbol{C})$ and an electromechanical (coupled) component, denoted as $\Psi_{em}(\boldsymbol{C}, \boldsymbol{E}_0)$ [30], namely

$$\Psi(\boldsymbol{C}, \boldsymbol{E}_0) = \Psi_m(\boldsymbol{C}) + \Psi_{em}(\boldsymbol{C}, \boldsymbol{E}_0). \tag{8}$$

From the additive decomposition of the free energy density $\Psi(\boldsymbol{C}, \boldsymbol{E}_0)$ in Equation (8), the PK2 stress tensor can be derived by taking derivatives of $\Psi(\boldsymbol{C}, \boldsymbol{E}_0)$ with respect to the right Cauchy-Green tensor, namely

$$\boldsymbol{S} = 2\frac{\partial \Psi\left(\boldsymbol{C}, \boldsymbol{E}_0\right)}{\partial \boldsymbol{C}} = 2\frac{\partial \Psi_m(\boldsymbol{C})}{\partial \boldsymbol{C}} + 2\frac{\partial \Psi_{em}\left(\boldsymbol{C}, \boldsymbol{E}_0\right)}{\partial \boldsymbol{C}} := \boldsymbol{S}_m + \boldsymbol{S}_{em},$$

where $\boldsymbol{S}_m$ is the mechanical part of the PK2 stress tensor and $\boldsymbol{S}_{em}$ is the electromechanical one. In addition, the Lagrangian electric displacement field $\boldsymbol{D}_0$ can be related with the Lagrangian electric field $\boldsymbol{E}_0$ through the free energy density as follows:

$$\boldsymbol{D}_0 = -\frac{\partial \Psi(\boldsymbol{C}, \boldsymbol{E}_0)}{\partial \boldsymbol{E}_0} = -\frac{\partial \Psi_{em}(\boldsymbol{C}, \boldsymbol{E}_0)}{\partial \boldsymbol{E}_0}.$$

Without loss of generality, we will consider in this study $\Psi_{em}(\boldsymbol{C}, \boldsymbol{E}_0)$ to represent an ideal dielectric elastomer, defined as follows [30]

$$\Psi_{em}(\boldsymbol{C}, \boldsymbol{E}_0) = -\frac{\varepsilon}{2} J \boldsymbol{E}_0 \cdot \boldsymbol{C}^{-1} \cdot \boldsymbol{E}_0, \tag{9}$$

where ε is the electric permittivity of the dielectric and $\boldsymbol{C}^{-1} = \boldsymbol{F}^{-1} \cdot \boldsymbol{F}^{-\mathrm{T}}$ is the inverse right Cauchy-Green tensor.

The main goal of this work is to study finite strain electromechanics, including the incompressible limit. The volumetric/deviatoric split of the mechanical part of the PK2 stress tensor is the starting point to develop mixed formulations capable of dealing with these physical problems [58, 59]. Although in principle this split can be performed on the entire stress field $\boldsymbol{S} = \boldsymbol{S}_m + \boldsymbol{S}_{em}$, it can also be applied just on the mechanical component of $\boldsymbol{S}$, namely

$$\boldsymbol{S}_m = \boldsymbol{S}' - pJ\boldsymbol{C}^{-1}, \tag{10}$$

where $\boldsymbol{S}'$ represents the deviatoric PK2 mechanical stress tensor (see Remark 3.3 below) and p is the pressure field of the mechanical stress tensor. We aim to address compressible models that can reach the incompressible limit. To characterize these models effectively, it is customary to use a decoupled representation of the purely mechanical strain energy density in the following specific form

$$\Psi_m(\boldsymbol{C}) = \Psi'_m(\overline{\boldsymbol{C}}) + \Psi^{vol}_m(J),$$

where $\overline{\boldsymbol{C}} = J^{-2/3}\boldsymbol{C}$ is the volume-preserving part of $\boldsymbol{C}$. Let us remark that this decomposition allows one to split the purely mechanical response of the material into the so-called deviatoric and volumetric parts, respectively, measured in the initial configuration. We can now derive the mechanical part of the PK2 stress tensor according to this split as

$$\boldsymbol{S}_m = 2\frac{\partial \Psi_m}{\partial \boldsymbol{C}} = 2\frac{\partial \Psi'_m}{\partial \boldsymbol{C}} + 2\frac{\partial \Psi^{vol}_m}{\partial \boldsymbol{C}} = 2\frac{\partial \Psi'_m}{\partial \boldsymbol{C}} + \frac{d\Psi^{vol}_m}{dJ} J\boldsymbol{C}^{-1}.$$

By comparing this definition with Equation (10) we obtain expressions for both the pressure and the deviatoric PK2 mechanical stress

$$\boldsymbol{S}' = 2\frac{\partial \Psi'_m}{\partial \boldsymbol{C}} \quad \text{and} \quad p = -\frac{d\Psi^{vol}_m}{dJ}. \tag{11}$$

Several constitutive models for both deviatoric and volumetric components are shown in [58]. Let us just describe the ones that will be applied in this work. Readers are referred to [14, 48] for further details on this kind of model.

3.4.1 | Deviatoric Models

The strain energy density must be written in terms of the strain invariants, which are defined for the volume-preserving $\overline{\boldsymbol{C}}$ by

$$\bar{I}_1 = \text{trace } \overline{\boldsymbol{C}}, \quad \bar{I}_2 = \frac{1}{2}\left[(\text{trace } \overline{\boldsymbol{C}})^2 - \text{trace}\left(\overline{\boldsymbol{C}}^2\right)\right] = \text{trace Cof } \boldsymbol{C},$$

where Cof $\boldsymbol{C}$ represents the cofactor of $\boldsymbol{C}$, and can be obtained as

$$\text{Cof}\,\boldsymbol{C} = J^2\boldsymbol{C}^{-1} = \frac{1}{2}\boldsymbol{C} \times \boldsymbol{C},$$

where the tensor cross product operation $\bullet \times \bullet$ between second-order tensors has been defined in Section 2.1

Let us present two suitable functions for the deviatoric component of the strain energy function:

- *Neo-Hookean model*:
  This model results from considering only the first principal invariant

$$\Psi'_m(\bar{I}_1) = \frac{\mu}{2}(\bar{I}_1 - 3), \tag{12}$$

  where $\mu > 0$ is the shear modulus.

- *Mooney-Rivlin model*:
  This model is derived considering the dependence on the second invariant as

$$\Psi'_m(\bar{I}_1, \bar{I}_2) = \alpha_1(\bar{I}_1 - 3) + \alpha_2(\bar{I}_2 - 3), \tag{13}$$

  where α_1 and α_2 are material parameters that must satisfy $\mu = 2(\alpha_1 + \alpha_2) > 0$.

3.4.2 | Volumetric Models

Due to the decoupled form of the mechanical strain energy density, compressibility of the mechanical contribution is accounted for by the volumetric strain energy function. Let us now show two models which depend upon the bulk modulus $\kappa = \frac{2\mu(1+\nu)}{3(1-2\nu)}$, where ν is the Poisson ratio.

- Quadratic [68]

$$\Psi_m^{vol}(J) = \frac{\kappa}{2}(J-1)^2; \quad \frac{d\Psi_m^{vol}}{dJ} = \kappa(J-1). \tag{14}$$

- Simo-Taylor [69]

$$\Psi_m^{vol}(J) = \frac{\kappa}{4}\left(J^2 - 1 - 2\log\ J\right); \quad \frac{d\Psi_m^{\text{vol}}}{dJ} = \frac{\kappa}{2}\left(J - \frac{1}{J}\right) = \frac{\kappa}{2}\left(\frac{J^2-1}{J}\right). \tag{15}$$

We can introduce the split of the PK2 mechanical stress tensor in the local conservation of linear momentum given in Equation (7a) to obtain its split version as

$$\begin{aligned} \nabla_0 \cdot \{\boldsymbol{F} \cdot \boldsymbol{S}_{em}\} - \nabla_0 \cdot \{\boldsymbol{F} \cdot \boldsymbol{S}'\} + \nabla_0 \cdot \{pJ\boldsymbol{F}^{-\mathrm{T}}\} &= \boldsymbol{f}_0 \qquad \text{in } V, \\ \{\boldsymbol{F} \cdot \boldsymbol{S}_{em} + \boldsymbol{F} \cdot \boldsymbol{S}' - pJ\boldsymbol{F}^{-\mathrm{T}}\} \cdot \boldsymbol{N} &= \boldsymbol{t}_0 \qquad \text{on } \partial V_{\mathrm{t}}, \\ \boldsymbol{u} &= \boldsymbol{u}_{\mathrm{D}} \qquad \text{on } \partial V_{\mathrm{u}}. \end{aligned}$$

Remark 3.1. The volumetric functions can be written as $\Psi_m^{vol}(J) = \kappa\hat{\Psi}_m^{vol}(J)$. Therefore, Equation (11) can be used to obtain a proper way to impose the incompressibility of a hyperelastic material

$$p = -\frac{d\Psi_m^{vol}}{dJ} \quad \Leftrightarrow \quad p = -\kappa\frac{d\hat{\Psi}_m^{vol}}{dJ} \quad \Leftrightarrow \quad \frac{p}{\kappa} + \frac{d\hat{\Psi}_m^{vol}}{dJ} = 0. \tag{16}$$

This equation can be applied regardless of the compressibility of the material under study. It is interesting to observe that in the incompressible limit, when Poisson's ratio $\nu \to 0.5$ (for isotropic materials), then $\kappa \to \infty$ and Equation (16) reduces automatically to

$$\frac{d\hat{\Psi}_m^{vol}}{dJ} = 0. \tag{17}$$

Equation (17) imposes directly that $J = 1$, which is in fact the condition that a material must satisfy to be incompressible in finite strain theory.

Remark 3.2. Although the volumetric contribution is typically not used in the fully incompressible case, the enforcement of the incompressibility constraint is not unique and admits infinitely many formulations. For example, it can be imposed via the condition $J - 1 = 0$, which corresponds to $\frac{d\hat{\Psi}_m^{vol}}{dJ} = 0$ for the volumetric strain energy function introduced in Equation (14). Alternatively, a more nonlinear form such as $(J^2 - 1)/J = 0$ may be adopted, which corresponds to $\frac{d\hat{\Psi}_m^{vol}}{dJ} = 0$ for the energy function in Equation (15).

Remark 3.3. Tensor $\boldsymbol{S}'$ is often referred to as the true deviatoric component of $\boldsymbol{S}_m$. However, it does not imply that the trace of $\boldsymbol{S}'$ must vanish. In fact, the 'true' deviatoric component of $\boldsymbol{S}_m$ satisfies the following equation (see for instance [70])

$$\boldsymbol{S}' : \boldsymbol{C} = 0,$$

which can be interpreted as the trace with respect to the metric tensor $\boldsymbol{C}$. The above equation enables the mechanic pressure p to be evaluated directly from $\boldsymbol{S}_m$ as

$$p = \frac{1}{3J}\boldsymbol{S}_m : \boldsymbol{C}.$$

Remark 3.4. It is important to note that, although we refer to p as pressure, it should not be identified as the hydrostatic pressure. In this case, p is characterized by the volumetric/deviatoric decomposition of the mechanical component of the PK2 stress tensor, $\boldsymbol{S}_m$ given in Equation (10). However, the electromechanical part remains. To define the hydrostatic pressure, we would need to decompose $\boldsymbol{S}_{em}$ into its deviatoric and volumetric components

$$\boldsymbol{S}_{em} = \boldsymbol{S}'_{em} - p_{em} J \boldsymbol{C}^{-1},$$

and the hydrostatic pressure would be recognized as $p_{hyd} = p + p_{em}$.

Remark 3.5. As an alternative to the free energy density $\Psi(\boldsymbol{C}, \boldsymbol{E}_0)$, some authors utilize the internal energy density $e(\boldsymbol{C}, \boldsymbol{D}_0)$. These two energy densities are connected via the following partial Legendre transformation:

$$\Psi(\boldsymbol{C}, \boldsymbol{E}_0) = -\sup_{\boldsymbol{D}_0}\{\boldsymbol{E}_0 \cdot \boldsymbol{D}_0 - e(\boldsymbol{C}, \boldsymbol{D}_0)\}. \tag{18}$$

In [30, 31], the authors proposed an extension of the concepts of rank-one convexity and polyconvexity [41] from hyperelasticity [33, 71, 72] to the domain of nonlinear electromechanics. They postulated an extended representation of the internal energy given by:

$$e(\boldsymbol{C}, \boldsymbol{D}_0) = \mathbb{W}\big(\boldsymbol{F}, \mathrm{Cof}\, \boldsymbol{F}, J, \boldsymbol{D}_0, \boldsymbol{F} \cdot \boldsymbol{D}_0\big),$$

which must be convex with respect to its five arguments to guarantee existence of minimizers and material stability in the context of electromechanics [32]. Notice that for the electromechanical model chosen in this work, in Equation (9), its associated internal energy density (reversing the Legendre transformation in Equation (18)) is indeed

$$\Psi_{em}(\boldsymbol{C}, \boldsymbol{E}_0) = -\frac{\varepsilon}{2} J \boldsymbol{E}_0 \cdot \boldsymbol{C}^{-1} \cdot \boldsymbol{E}_0 \Rightarrow e_{em}(\boldsymbol{C}, \boldsymbol{D}_0) = \frac{\varepsilon}{2} J^{-1} \boldsymbol{D}_0 \cdot \boldsymbol{C} \cdot \boldsymbol{D}_0 = \frac{\varepsilon}{2} J^{-1}\big(\boldsymbol{F} \cdot \boldsymbol{D}_0\big) \cdot \big(\boldsymbol{F} \cdot \boldsymbol{D}_0\big). \tag{19}$$

The last expression in Equation (19) is indeed convex (provided that $J > 0$) with respect to the two fields $\{J, \boldsymbol{F} \cdot \boldsymbol{D}_0\}$ simultaneously (see [30]), thereby satisfying the definition of polyconvexity in electromechanics. For the isochoric mechanical contribution, the Neo-Hookean model $\Psi'_m(\bar{I}_1)$ in Equation (12) is convex simultaneously with respect to $\{\boldsymbol{F}, J\}$. The isochoric Mooney-Rivlin model $\Psi'_m(\bar{I}_1, \bar{I}_2)$ in Equation (13), specifically the second term depending linearly upon $\bar{I}_2$ is not polyconvex, that is, is not convex with respect to $\{J, \mathrm{Cof}\, \boldsymbol{F}\}$. This issue can be addressed by considering the polyconvex invariant $\bar{I}_2^n$, with $n \geq 3/2$. Nonetheless, despite its non-polyconvexity, $\bar{I}_2$ remains widely used, and we will employ it in our numerical simulations. Importantly, we have not observed any material instability linked to a potential loss of rank-one convexity in the overall free energy density due to this term. Finally, both volumetric terms $\Psi_m^{\mathrm{vol}}(J)$ in Equations (14) and (15) are convex with respect to J, hence polyconvex.

3.5 | Electromechanics: Governing Equations

In this subsection, the entire set of governing equations in finite strain electromechanics is presented. To do so, the local form of Faraday's and Gauss's laws introduced in Subsection 3.3 are considered in combination with the conservation of linear momentum detailed in Section 3.2. Furthermore, the constitutive model described in Section 3.4 is also considered to close the system of equations by relating deformation and electric displacements to stresses and electric fields in the continuum. The governing equations in finite strain electromechanics are:

$$-\boldsymbol{\nabla}_0 \cdot \{\boldsymbol{F} \cdot \boldsymbol{S}_{em}\} - \boldsymbol{\nabla}_0 \cdot \{\boldsymbol{F} \cdot \boldsymbol{S}'\} + \boldsymbol{\nabla}_0 \cdot \{p J \boldsymbol{F}^{-\mathrm{T}}\} = \boldsymbol{f}_0 \qquad \text{in } V, \tag{20a}$$

$$\frac{p}{\kappa} + \frac{d\hat{\Psi}_m^{vol}}{dJ} = 0 \qquad \text{in } V, \tag{20b}$$

$$\boldsymbol{S}' - 2\frac{\partial \Psi'_m}{\partial \boldsymbol{C}} = \boldsymbol{0} \qquad \text{in } V, \tag{20c}$$

$$\boldsymbol{S}_{em} - 2\frac{\partial \Psi_{em}}{\partial \boldsymbol{C}} = \boldsymbol{0} \qquad \text{in } V, \tag{20d}$$

$$\boldsymbol{\nabla}_0 \cdot \boldsymbol{D}_0 = \rho_0^{\mathrm{e}} \qquad \text{in } V, \tag{20e}$$

$$\boldsymbol{E}_0 + \boldsymbol{\nabla}_0 \varphi = \boldsymbol{0} \qquad \text{in } V, \tag{20f}$$

$$\boldsymbol{D}_0 + \frac{\partial \Psi_{em}}{\partial \boldsymbol{E}_0} = \boldsymbol{0} \qquad \text{in } V, \tag{20g}$$

$$\{\boldsymbol{F} \cdot \boldsymbol{S}_{em} + \boldsymbol{F} \cdot \boldsymbol{S}' - pJ\boldsymbol{F}^{-\mathrm{T}}\} \cdot \boldsymbol{N} = \boldsymbol{t}_0 \qquad \text{on } \partial V_{\mathrm{t}}, \tag{20h}$$

$$\boldsymbol{u} = \boldsymbol{u}_{\mathrm{D}} \qquad \text{on } \partial V_{\mathrm{u}}, \tag{20i}$$

$$\boldsymbol{D}_0 \cdot \boldsymbol{N} = -\omega_0^{\mathrm{e}} \qquad \text{on } \partial V_{\omega}, \tag{20j}$$

$$\varphi = \varphi_{\mathrm{D}} \qquad \text{on } \partial V_{\varphi}. \tag{20k}$$

The irreducible formulation, where displacements and electric potential fields are considered as the primary variables of the problem, cannot be applied to this type of coupled problem. This formulation inherits volumetric, shear, and torsional locking issues from displacement-based formulations in nonlinear solid mechanics, with the constitutive matrix approaching singularity in the incompressible limit [58, 59]. To address this issue, this work presents two novel mixed formulations that introduce the pressure as an extra unknown in the problem, allowing us to properly handle the incompressible limit.

4 | Stabilized Mixed Formulations for Electromechanics

In this section, two different mixed formulations are considered to manage the problem described above: On the one hand, the mixed three-field $\boldsymbol{u}p\varphi$ formulation, in which the addition of the pressure field as an extra primary variable with respect to the standard displacement-electric potential based formulation is considered to be able to enforce the incompressibility constraint; on the other hand, a mixed four-field $\boldsymbol{u}p\boldsymbol{S}'\varphi$ formulation, in which the deviatoric PK2 mechanical stress tensor is added as unknown of the problem. The final goal is to design an FE technology able to tackle simultaneously problems which may involve incompressible behavior together with a high degree of accuracy of the stress field, as well as a robust behavior in solids with a very thin geometrical dimension [73, 74].

4.1 | The $up\varphi$ Formulation

4.1.1 | Governing Equations

The first formulation we consider is the mixed three-field $\boldsymbol{u}p\varphi$ formulation, which is introduced to deal with nearly and fully incompressible materials. The problem consists of finding a displacement $\boldsymbol{u} : V \to \mathbb{R}^d$, a pressure $p : V \to \mathbb{R}$ and an electric potential $\varphi : V \to \mathbb{R}$ such that

$$\boldsymbol{\nabla}_0 \cdot \{\boldsymbol{F} \cdot \boldsymbol{S}_{em}\} - \boldsymbol{\nabla}_0 \cdot \{\boldsymbol{F} \cdot \boldsymbol{S}'\} + \boldsymbol{\nabla}_0 \cdot \{pJ\boldsymbol{F}^{-\mathrm{T}}\} = \boldsymbol{f}_0 \qquad \text{in } V, \tag{21a}$$

$$\frac{p}{\kappa} + \frac{d\hat{\Psi}_m^{vol}}{dJ} = 0 \qquad \text{in } V, \tag{21b}$$

$$\boldsymbol{\nabla}_0 \cdot \boldsymbol{D}_0 = \rho_0^{\mathrm{e}} \qquad \text{in } V, \tag{21c}$$

where $\boldsymbol{F}$, $\boldsymbol{S}'$, J and $\frac{d\hat{\Psi}_m^{vol}}{dJ}$ are functions of the displacement field and $\boldsymbol{S}_{em}$ and $\boldsymbol{D}_0$ are functions of both the displacement field and the electric potential. The problem must be supplied with the already-defined boundary conditions.

4.1.2 | Variational Formulation

Let $\mathcal{V}$, $\mathcal{Q}$, and $\mathcal{N}$ be, respectively, the proper functional spaces where displacement, pressure, and electric potential solutions are well-defined. We denote by $\mathcal{V}_0$ functions in $\mathcal{V}$ which vanish on the boundary ∂V_u and by $\mathcal{N}_0$ functions in $\mathcal{N}$ which vanish on the boundary ∂V_{φ}. We shall be interested also in the spaces $\mathcal{W} := \mathcal{V} \times \mathcal{Q} \times \mathcal{N}$ and $\mathcal{W}_0 := \mathcal{V}_0 \times \mathcal{Q} \times \mathcal{N}_0$.

The variational statement of the problem is derived by testing system (21) against arbitrary test functions, $\boldsymbol{V} := [\boldsymbol{v}, q, \eta]^T$, $\boldsymbol{v} \in \mathcal{V}_0$, $q \in \mathcal{Q}$ and $\eta \in \mathcal{N}_0$. At load increment n, the weak form of the problem reads: Find $\boldsymbol{U}^n := [\boldsymbol{u}^n, p^n, \varphi^n]^T \in \mathcal{W}$ such that the Dirichlet conditions are satisfied and

$$A_{\boldsymbol{u}p\varphi}(\boldsymbol{V}, \boldsymbol{U}^n) = \lambda^n F(\boldsymbol{V}) \quad \forall \boldsymbol{V} \in \mathcal{W}_0 \,, \tag{22}$$

where $A_{\boldsymbol{u}p\varphi}(\boldsymbol{V}, \boldsymbol{U})$ is a semilinear form defined on $\mathcal{W}_0 \times \mathcal{W}$ as

$$A_{\boldsymbol{u}p\varphi}(\boldsymbol{V}, \boldsymbol{U}) := \langle \boldsymbol{\nabla}_0 \boldsymbol{v}, \boldsymbol{F} \cdot \boldsymbol{S}_{em} \rangle + \left\langle \boldsymbol{\nabla}_0 \boldsymbol{v}, \boldsymbol{F} \cdot \boldsymbol{S}' \right\rangle - \left\langle \boldsymbol{\nabla}_0 \boldsymbol{v}, pJ\boldsymbol{F}^{-\mathrm{T}} \right\rangle + \left\langle q, \frac{d\hat{\Psi}^{vol}_m}{dJ} \right\rangle + \left\langle q, \frac{p}{\kappa} \right\rangle - \langle \boldsymbol{\nabla}_0 \eta, \boldsymbol{D}_0 \rangle.$$

$F(\boldsymbol{V})$ is a linear form defined on $\mathcal{W}_0$ as

$$F(\boldsymbol{V}) := \langle \boldsymbol{v}, \boldsymbol{f}_0 \rangle + \langle \boldsymbol{v}, \boldsymbol{t}_0 \rangle_{\partial V_t} + \left\langle \eta, \rho_0^{\mathrm{e}} \right\rangle - \left\langle \eta, \omega_0^{\mathrm{e}} \right\rangle_{\partial V_\omega}. \tag{23}$$

4.1.3 | Linearization

To solve the problem, the system needs to be linearized so that a bilinear operator, which allows us to compute a correction $\boldsymbol{\delta U}$ of a given guess for the solution, is obtained, which we denote by $\boldsymbol{U}$. As it is explained in Section 5, iterations until convergence will be performed for each load increment. Thus, the unknown $\boldsymbol{U}^n$ could be written at the ith iteration as $\boldsymbol{U}^{n,i} = \boldsymbol{U}^{n,i-1} + \boldsymbol{\delta U}^{n,i}$, the first superscript denoting the load increment and the second the iteration counter. However, load and iteration counters of the given guess and the increment will be omitted to simplify the notation, and we will simply write $\boldsymbol{U}^{n,i} = \boldsymbol{U} + \boldsymbol{\delta U}$.

After using a Newton-Raphson scheme, we obtain the following linearized form of the problem. Given $\boldsymbol{U}$ as the guess for the solution at the previous iteration and at load increment n, find a correction $\boldsymbol{\delta U} := [\boldsymbol{\delta u}, \delta p, \delta\varphi]^T \in \mathcal{W}_0$ such that

$$B_{\boldsymbol{u}p\varphi}(\boldsymbol{U}; \boldsymbol{V}, \boldsymbol{\delta U}) = \lambda^n F(\boldsymbol{V}) - A_{\boldsymbol{u}p\varphi}(\boldsymbol{V}, \boldsymbol{U}) \quad \forall \boldsymbol{V} \in \mathcal{W}_0 \,, \tag{24}$$

where $B_{\boldsymbol{u}p\varphi}(\boldsymbol{U}; \boldsymbol{V}, \boldsymbol{\delta U})$ is the bilinear form obtained through the Newton-Raphson linearization, and it is defined on $\mathcal{W}_0 \times \mathcal{W}_0$ as

$$\begin{aligned} B_{\boldsymbol{u}p\varphi}(\boldsymbol{U}; \boldsymbol{V}, \boldsymbol{\delta U}) := {} & \langle \boldsymbol{\nabla}_0 \boldsymbol{v}, \boldsymbol{\nabla}_0 \boldsymbol{\delta u} \cdot \boldsymbol{S}_{em} \rangle + \left\langle \boldsymbol{F}^T \cdot \boldsymbol{\nabla}_0 \boldsymbol{v}, \mathbb{C}_{em} : \left(\boldsymbol{F}^T \cdot \boldsymbol{\nabla}_0 \boldsymbol{\delta u} \right) \right\rangle + \left\langle \boldsymbol{F}^T \cdot \boldsymbol{\nabla}_0 \boldsymbol{v}, \mathbb{P}_{em} \cdot \boldsymbol{\nabla}_0 \delta\varphi \right\rangle + \left\langle \boldsymbol{\nabla}_0 \boldsymbol{v}, \boldsymbol{\nabla}_0 \boldsymbol{\delta u} \cdot \boldsymbol{S}' \right\rangle \\ & + \left\langle \boldsymbol{F}^T \cdot \boldsymbol{\nabla}_0 \boldsymbol{v}, \mathbb{C}' : \left(\boldsymbol{F}^T \cdot \boldsymbol{\nabla}_0 \boldsymbol{\delta u} \right) \right\rangle - \left\langle \boldsymbol{\nabla}_0 \boldsymbol{v}, Jp\left(\boldsymbol{\nabla}_0 \boldsymbol{\delta u} : \boldsymbol{F}^{-1} \right) \boldsymbol{F}^{-T} \right\rangle + \left\langle \boldsymbol{\nabla}_0 \boldsymbol{v}, Jp\left(\boldsymbol{F}^{-1} \cdot \boldsymbol{\nabla}_0 \boldsymbol{\delta u} \cdot \boldsymbol{F}^{-1} \right)^T \right\rangle \\ & - \left\langle \boldsymbol{\nabla}_0 \boldsymbol{v}, \delta p J \boldsymbol{F}^{-\mathrm{T}} \right\rangle + \left\langle q, J \frac{d^2\hat{\Psi}^{vol}_m}{dJ^2} \boldsymbol{\nabla}_0 \boldsymbol{\delta u} : \boldsymbol{F}^{-T} \right\rangle + \left\langle q, \frac{\delta p}{\kappa} \right\rangle - \left\langle \boldsymbol{\nabla}_0 \eta, \mathbb{P}_{em} : \left(\boldsymbol{F}^T \cdot \boldsymbol{\nabla}_0 \boldsymbol{\delta u} \right) \right\rangle \\ & + \langle \boldsymbol{\nabla}_0 \eta, \mathbb{E}_{em} \cdot \boldsymbol{\nabla}_0 \delta\varphi \rangle, \end{aligned} \tag{25}$$

where in Equation (25) it is understood that all the tensors involved are computed with the given guess $\boldsymbol{U}$.

From the linearization of the stresses, there appear the fourth-order electromechanic tensor $\mathbb{C}_{em}$, the deviatoric part of the fourth-order elastic tensor $\mathbb{C}'$, the third-order piezoelectric tensor $\mathbb{P}_{em}$, and the second-order dielectric tensor $\mathbb{E}_{em}$ defined as

$$\mathbb{C}_{em} = 4\frac{\partial^2 \Psi_{em}(\boldsymbol{C}, \boldsymbol{E}_0)}{\partial \boldsymbol{C}\, \partial \boldsymbol{C}}; \; \mathbb{C}' = 4\frac{\partial^2 \Psi'_m(\boldsymbol{C})}{\partial \boldsymbol{C}\, \partial \boldsymbol{C}}; \; \mathbb{P}_{em} = -2\frac{\partial^2 \Psi_{em}(\boldsymbol{C}, \boldsymbol{E}_0)}{\partial \boldsymbol{C}\, \partial \boldsymbol{E}_0}; \; \mathbb{E}_{em} = -\frac{\partial^2 \Psi_{em}(\boldsymbol{C}, \boldsymbol{E}_0)}{\partial \boldsymbol{E}_0\, \partial \boldsymbol{E}_0}.$$

These tensors are also evaluated with the given guess $\boldsymbol{U}$.

4.1.4 | Symmetrization

The symmetric form of the problem can be defined as

$$B^{sym}_{\boldsymbol{u}p\varphi}(\boldsymbol{U}; \boldsymbol{V}, \boldsymbol{\delta U}) = \lambda^n F(\boldsymbol{V}) - A^{\mathrm{sym}}_{\boldsymbol{u}p\varphi}(\boldsymbol{V}, \boldsymbol{U}) \quad \forall \boldsymbol{V} \in \mathcal{W}_0, \tag{26}$$

where

$$
\begin{aligned}
B^{\mathrm{sym}}_{\boldsymbol{u}p\varphi}(\boldsymbol{U};\boldsymbol{V},\boldsymbol{\delta U}) :=\ & \langle \boldsymbol{\nabla}_0\boldsymbol{v}, \boldsymbol{\nabla}_0\boldsymbol{\delta u}\cdot\boldsymbol{S}_{em}\rangle + \left\langle \boldsymbol{F}^T\cdot\boldsymbol{\nabla}_0\boldsymbol{v}, \mathbb{C}_{em} : \left(\boldsymbol{F}^T\cdot\boldsymbol{\nabla}_0\boldsymbol{\delta u}\right)\right\rangle + \left\langle \boldsymbol{F}^T\cdot\boldsymbol{\nabla}_0\boldsymbol{v}, \mathbb{P}_{em}\cdot\boldsymbol{\nabla}_0\delta\varphi\right\rangle + \left\langle \boldsymbol{\nabla}_0\boldsymbol{v}, \boldsymbol{\nabla}_0\boldsymbol{\delta u}\cdot\boldsymbol{S}'\right\rangle \\
&+ \left\langle \boldsymbol{F}^T\cdot\boldsymbol{\nabla}_0\boldsymbol{v}, \mathbb{C}' : \left(\boldsymbol{F}^T\cdot\boldsymbol{\nabla}_0\boldsymbol{\delta u}\right)\right\rangle - \left\langle \boldsymbol{\nabla}_0\boldsymbol{v}, Jp\left(\boldsymbol{\nabla}_0\boldsymbol{\delta u} : \boldsymbol{F}^{-1}\right)\boldsymbol{F}^{-T}\right\rangle + \left\langle \boldsymbol{\nabla}_0\boldsymbol{v}, Jp\left(\boldsymbol{F}^{-1}\cdot\boldsymbol{\nabla}_0\boldsymbol{\delta u}\cdot\boldsymbol{F}^{-1}\right)^T\right\rangle \\
&- \left\langle \boldsymbol{\nabla}_0\boldsymbol{v}, \delta pJ\boldsymbol{F}^{-\mathrm{T}}\right\rangle + \left\langle q, J\boldsymbol{\nabla}_0\boldsymbol{\delta u} : \boldsymbol{F}^{-T}\right\rangle + \left\langle q, \left(\frac{d^2\hat{\Psi}^{vol}_m}{dJ^2}\right)^{-1}\frac{\delta p}{\kappa}\right\rangle - \left\langle \boldsymbol{\nabla}_0\eta, \mathbb{P}_{em} : \left(\boldsymbol{F}^T\cdot\boldsymbol{\nabla}_0\boldsymbol{\delta u}\right)\right\rangle \\
&+ \langle \boldsymbol{\nabla}_0\eta, \mathbb{E}_{em}\cdot\boldsymbol{\nabla}_0\delta\varphi\rangle, \\
A^{\mathrm{sym}}_{\boldsymbol{u}p\varphi}(\boldsymbol{V},\boldsymbol{U}) :=\ & \langle \boldsymbol{\nabla}_0\boldsymbol{v}, \boldsymbol{F}\cdot\boldsymbol{S}_{em}\rangle + \left\langle \boldsymbol{\nabla}_0\boldsymbol{v}, \boldsymbol{F}\cdot\boldsymbol{S}'\right\rangle - \left\langle \boldsymbol{\nabla}_0\boldsymbol{v}, pJ\boldsymbol{F}^{-\mathrm{T}}\right\rangle + \left\langle q, \left(\frac{d^2\hat{\Psi}^{vol}_m}{dJ^2}\right)^{-1}\frac{d\hat{\Psi}^{vol}_m}{dJ}\right\rangle + \left\langle q, \left(\frac{d^2\hat{\Psi}^{vol}_m}{dJ^2}\right)^{-1}\frac{p}{\kappa}\right\rangle \\
&- \langle \boldsymbol{\nabla}_0\eta, \boldsymbol{D}_0\rangle,
\end{aligned}
$$

where we have multiplied the second equation by the linearized term $\left(\frac{d^2\hat{\Psi}^{vol}_m}{dJ^2}\right)^{-1}$. Note that to obtain a truly symmetric problem, δp should be replaced by $-\delta p$; we maintain this expression to highlight the positivity of the term involving κ^{-1}.

The symmetric form of the problem can be interesting from both the theoretical and the practical points of view. From the theoretical point of view, the problem to be solved corresponds to the minimization of a certain electromechanical energy, whereas from the practical point of view, the symmetry can be exploited when solving the linear system. For simplicity, we will employ the non-symmetric form of the problem in what follows, although the use of the symmetric version would be straightforward.

4.1.5 | Galerkin Spatial Discretization

The Galerkin discrete version of problem (24) is: For a given load increment λ^n and a fixed iteration, find $\boldsymbol{\delta U}_h := \left[\boldsymbol{\delta u}_h, \delta p_h, \delta\varphi_h\right]^T \in \mathcal{W}_{h,0}$ such that

$$
B_{\boldsymbol{u}p\varphi}\left(\boldsymbol{U}_h;\boldsymbol{V}_h,\boldsymbol{\delta U}_h\right) = \lambda^n F\left(\boldsymbol{V}_h\right) - A_{\boldsymbol{u}p\varphi}\left(\boldsymbol{V}_h,\boldsymbol{U}_h\right) \quad \forall \boldsymbol{V}_h \in \mathcal{W}_{h,0}.
$$

The stability of the discrete formulation depends on compatibility restrictions on the interpolation functions chosen for the displacement, pressure, and electric potential fields, as stated by the appropriate inf-sup condition [63]. According to these restrictions, mixed elements with continuous equal-order linear interpolation for all fields are not stable. However, the inf-sup condition can be circumvented by using a stabilization technique. This is why the so-called stabilized formulations have been proposed to approximate these kinds of problems. The main idea is to replace Equation (24) by another discrete variational problem in which the bilinear form $B_{\boldsymbol{u}p\varphi}$ is enhanced so that it has improved stability properties. To overcome the instabilities previously discussed, we propose the stabilization technique described in Section 2.5.

Remark 4.1. Let us consider now the symmetrized problem (26) and discuss the stability of this linearized problem; again, the discussion could be extended to the original nonlinear problem. Taking $\boldsymbol{v}_h = \boldsymbol{\delta u}_h$, $\eta_h = \delta\varphi_h$ (assuming homogeneous Dirichlet boundary conditions) and $q_h = \delta p_h$ it is found that

$$
\begin{aligned}
B^{\mathrm{sym}}_{\boldsymbol{u}p\varphi}\left(\boldsymbol{U}_h;\boldsymbol{\delta U}_h,\boldsymbol{\delta U}_h\right) :=\ & \langle \boldsymbol{\nabla}_0\boldsymbol{\delta u}_h, \boldsymbol{\nabla}_0\boldsymbol{\delta u}_h\cdot\boldsymbol{S}_{em}\rangle + \left\langle \boldsymbol{F}^T\cdot\boldsymbol{\nabla}_0\boldsymbol{\delta u}_h, \mathbb{C}_{em} : \left(\boldsymbol{F}^T\cdot\boldsymbol{\nabla}_0\boldsymbol{\delta u}_h\right)\right\rangle \\
&+ \left\langle \boldsymbol{\nabla}_0\boldsymbol{\delta u}_h, \boldsymbol{\nabla}_0\boldsymbol{\delta u}_h\cdot\boldsymbol{S}'\right\rangle + \left\langle \boldsymbol{F}^T\cdot\boldsymbol{\nabla}_0\boldsymbol{\delta u}_h, \mathbb{C}' : \left(\boldsymbol{F}^T\cdot\boldsymbol{\nabla}_0\boldsymbol{\delta u}_h\right)\right\rangle - \left\langle \boldsymbol{\nabla}_0\boldsymbol{\delta u}_h, Jp_h\left(\boldsymbol{\nabla}_0\boldsymbol{\delta u}_h : \boldsymbol{F}^{-1}\right)\boldsymbol{F}^{-T}\right\rangle \\
&+ \left\langle \boldsymbol{\nabla}_0\boldsymbol{\delta u}_h, Jp_h\left(\boldsymbol{F}^{-1}\cdot\boldsymbol{\nabla}_0\boldsymbol{\delta u}_h\cdot\boldsymbol{F}^{-1}\right)^T\right\rangle + \left\langle \delta p_h, \left(\frac{d^2\hat{\Psi}^{vol}_m}{dJ^2}\right)^{-1}\frac{\delta p_h}{\kappa}\right\rangle + \langle \boldsymbol{\nabla}_0\delta\varphi_h, \mathbb{E}_{em}\cdot\boldsymbol{\nabla}_0\delta\varphi_h\rangle.
\end{aligned}
$$

Suppose that the given guess is away from buckling, so that the solution of the continuous problem exists and is unique. Under this scenario, $\mathbb{C}'$ is a positive-definite tensor, and the fourth term including it provides control on the increment of the displacement field $\delta\boldsymbol{u}_h$. Furthermore, the second-order tensor $\mathbb{E}_{em}$ is also a positive-definite tensor, and hence, the last term allows us to have control over the increment of the electric potential field $\delta\varphi_h$. However, it is obvious that in the

nearly and fully incompressible cases, when $\kappa \to \infty$, the increment of pressure δp_h is out of control. The only possibility to have control over the pressure field is to satisfy the inf-sup condition

$$\inf_{q_h \in \mathcal{Q}_h} \sup_{\boldsymbol{v}_h \in \mathcal{V}_h} \frac{\langle \boldsymbol{\nabla} q_h, \boldsymbol{v}_h \rangle}{\|q_h\|_{\mathcal{Q}} \|\boldsymbol{v}_h\|_{\mathcal{V}}} \geq \beta_1 \tag{27}$$

for a constant $\beta_1 > 0$. Under appropriate conditions on the coupling, the proximity of the guess $\boldsymbol{U}_h$ to the solution $\boldsymbol{U}_h^n$ and the tensors $\mathbb{C}_{em}$, $\boldsymbol{S}_{em}$ and $\boldsymbol{S}'$, this has to allow one to prove that the global inf-sup condition of the problem, which can be written as

$$\inf_{\delta \boldsymbol{U}_h \in \mathcal{W}_{h,0}} \sup_{\boldsymbol{V}_h \in \mathcal{W}_{h,0}} \frac{B_{\boldsymbol{upp\varphi}}^{sym}(\boldsymbol{U}_h; \boldsymbol{V}_h, \delta \boldsymbol{U}_h)}{\|\boldsymbol{V}_h\|_{\mathcal{W}} \|\delta \boldsymbol{U}_h\|_{\mathcal{W}}} \geq \beta_2,$$

will be satisfied for a constant $\beta_2 > 0$. However, FE element interpolations satisfying the compatibility condition in Equation (27) are not convenient from the implementation point of view. In particular, it is not satisfied by the equal interpolation for all the unknowns, which is the approach we favor.

4.1.6 | Stabilized Formulation

According to the VMS framework explained in Section 2.5, the stabilized problem with S-OSGS is defined as

$$\begin{aligned} &B_{\boldsymbol{upp\varphi}}(\boldsymbol{U}_h; \boldsymbol{V}_h, \delta \boldsymbol{U}_h) + \sum_K \left\langle \hat{\mathscr{L}}^*_{\boldsymbol{upp\varphi}}(\boldsymbol{U}_h; \boldsymbol{V}_h), \boldsymbol{\tau}_K \cdot \tilde{\Pi}\left[\lambda^n f - \hat{\mathscr{A}}_{\boldsymbol{upp\varphi}}(\boldsymbol{U}_h) - \hat{\mathscr{L}}_{\boldsymbol{upp\varphi}}(\boldsymbol{U}_h; \delta \boldsymbol{U}_h)\right] \right\rangle_K \\ &\quad = \lambda^n F(\boldsymbol{V}_h) - A_{\boldsymbol{upp\varphi}}(\boldsymbol{V}_h, \boldsymbol{U}_h) \;\; \forall \boldsymbol{V}_h \in \mathcal{W}_{h,0}. \end{aligned}$$

Let us remark that $\boldsymbol{\tau}_K$ is taken as a diagonal matrix of stabilization parameters, $\boldsymbol{\tau}_K = \text{diag}(\tau_{\boldsymbol{u}} \boldsymbol{I}_d, 0)$, with $\boldsymbol{I}_d$ the identity on vectors of $\mathbb{R}^d$ and parameter $\tau_{\boldsymbol{u}}$ is a coefficient coming from the study of the behavior of the stabilization parameters based on a Fourier analysis of the problem for the SGSs. In this work, we propose to use the stabilization parameter presented in [58] for finite strain solid mechanics problems

$$\tau_{\boldsymbol{u}} = c_1 \frac{h_K^2}{2\mu} \tag{28}$$

where c_1 is an algorithmic parameter which must be determined. The split operators we need to define to have control over the pressure field are

$$\hat{\mathscr{A}}_{\boldsymbol{upp\varphi}}(\boldsymbol{U}) = \begin{bmatrix} \boldsymbol{\nabla}_0 \cdot \{pJ\boldsymbol{F}^{-\mathrm{T}}\} \\ 0 \end{bmatrix}, \qquad \hat{\mathscr{L}}^*_{\boldsymbol{upp\varphi}}(\boldsymbol{U}; \boldsymbol{V}) = \begin{bmatrix} -\boldsymbol{\nabla}_0 \cdot \left\{ qJ \frac{d^2 \hat{\Psi}_m^{vol}}{dJ^2} \boldsymbol{F}^{-\mathrm{T}} \right\} \\ 0 \end{bmatrix},$$

$$\hat{\mathscr{L}}_{\boldsymbol{upp\varphi}}(\boldsymbol{U}; \delta \boldsymbol{U}) = \begin{bmatrix} \boldsymbol{\nabla}_0 \cdot \left\{ -Jp(\boldsymbol{\nabla}_0 \delta \boldsymbol{u} : \boldsymbol{F}^{-1}) \boldsymbol{F}^{-T} + Jp(\boldsymbol{F}^{-1} \cdot \boldsymbol{\nabla}_0 \delta \boldsymbol{u} \cdot \boldsymbol{F}^{-1})^T + \delta p J \boldsymbol{F}^{-\mathrm{T}} \right\} \\ 0 \end{bmatrix}.$$

Thus, we introduce the term $\sum_K \tau_{\boldsymbol{u}} \left\langle \boldsymbol{\nabla}_0 \cdot \left\{ qJ \frac{d^2 \hat{\Psi}_m^{vol}}{dJ^2} \boldsymbol{F}^{-\mathrm{T}} \right\}, \tilde{\Pi}\left[\boldsymbol{\nabla}_0 \cdot \{\delta p J \boldsymbol{F}^{-\mathrm{T}}\}\right] \right\rangle_K$ on the left-hand side of the system, which provides control over the pressure gradient. This is enough to obtain control over the pressure itself when using continuous pressure interpolations, as we are considering. If one wishes to use discontinuous pressure interpolations, then inter-element boundary terms involving jumps of pressures need to be added, which can be understood as approximations to the SGSs on these boundaries (see [65]).

4.2 | The $upS'\varphi$ Formulation

4.2.1 | Governing Equations

The second formulation we consider is the mixed four-field $\boldsymbol{upS'\varphi}$ formulation. The objective of this formulation is the definition of a general framework, which includes the mixed $\boldsymbol{up\varphi}$ formulation presented in Section 4.1 to be able to tackle the incompressibility limit and introduces $\boldsymbol{S}'$ as primary unknown to obtain a higher accuracy in the computation of

stresses in finite strain problems, and also avoids possible locking when one of the dimensions of the body is small. The problem consists of finding a displacement $\boldsymbol{u} : V \to \mathbb{R}^d$, a pressure $p : V \to \mathbb{R}$, a deviatoric PK2 mechanical stress $\boldsymbol{S}' : V \to \mathbb{R}^d \otimes \mathbb{R}^d$ and an electric potential $\varphi : V \to \mathbb{R}$ such that

$$\boldsymbol{\nabla}_0 \cdot \{\boldsymbol{F} \cdot \boldsymbol{S}_{em}\} - \boldsymbol{\nabla}_0 \cdot \{\boldsymbol{F} \cdot \boldsymbol{S}'\} + \boldsymbol{\nabla}_0 \cdot \{pJ\boldsymbol{F}^{-\mathrm{T}}\} = \boldsymbol{f}_0 \qquad \text{in } V, \tag{29a}$$

$$\frac{p}{\kappa} + \frac{d\hat{\Psi}^{vol}_m}{dJ} = 0 \qquad \text{in } V, \tag{29b}$$

$$\boldsymbol{S}' - 2\frac{\partial \Psi'_m}{\partial \boldsymbol{C}} = \boldsymbol{0} \qquad \text{in } V, \tag{29c}$$

$$\boldsymbol{\nabla}_0 \cdot \boldsymbol{D}_0 = \rho_0^{\mathrm{e}} \qquad \text{in } V, \tag{29d}$$

where $\boldsymbol{F}$, J, and $\frac{d\hat{\Psi}^{vol}_m}{dJ}$ are functions of the displacement field and $\boldsymbol{S}_{em}$ and $\boldsymbol{D}_0$ are functions of both the displacement field and the electric potential. The problem must be supplied with the already-defined boundary conditions.

Remark 4.2. The motivation for introducing the mechanical deviatoric PK2 stress as a primary unknown lies in the need to improve the accuracy of the stress field representation in problems where shear and distortional effects play a dominant role. This is particularly relevant in the analysis of finite strain damage electromechanics, where capturing such effects is essential to accurately model material degradation and failure mechanisms. Notice that the incorporation of only the deviatoric component of the stress is sufficient to eliminate shear locking, which is one of the primary goals of this formulation, as clearly demonstrated by the performance of the $\boldsymbol{up}\boldsymbol{S}'\varphi$ approach in the numerical examples.

In viscoelasticity models, this component plays a fundamental role in describing time-dependent shear responses. The accurate representation of these stresses is especially important when dealing with stress concentrations, which could otherwise lead to numerical instabilities or convergence issues.

For design optimization problems, where total stresses are the primary variables of interest, it is indeed possible to reformulate the problem so that the total stress becomes the primary unknown. This would require a slight modification of the current formulation. However, in the context of this study, which is focused on capturing deviatoric effects and mechanical responses with high fidelity, we maintain that using the mechanical deviatoric PK2 stress as a primary variable is the most appropriate and effective approach.

4.2.2 | Variational Formulation

Let us consider the same spaces and test functions we have defined previously for the mixed $\boldsymbol{up}\varphi$ formulation. Let $\mathcal{T}$ be the proper functional space where the deviatoric PK2 mechanical stress components are well-defined. We shall be interested also in the spaces $\mathcal{W} := \mathcal{V} \times \mathcal{Q} \times \mathcal{T} \times \mathcal{N}$ and $\mathcal{W}_0 := \mathcal{V}_0 \times \mathcal{Q} \times \mathcal{T} \times \mathcal{N}_0$.

The variational statement of the problem is derived by testing system (29) against arbitrary test functions, $\boldsymbol{V} := [\boldsymbol{v}, q, \boldsymbol{T}, \eta]^T$, $\boldsymbol{v} \in \mathcal{V}_0$, $q \in \mathcal{Q}$, $\boldsymbol{T} \in \mathcal{T}$ and $\eta \in \mathcal{N}_0$. At load increment n, the weak form of the problem reads: find $\boldsymbol{U}^n := \left[\boldsymbol{u}^n, p^n, \boldsymbol{S}'^n, \varphi^n\right]^T \in \mathcal{W}$ such that the Dirichlet conditions are satisfied and

$$A_{\boldsymbol{up}\boldsymbol{S}'\varphi}(\boldsymbol{V}, \boldsymbol{U}^n) = \lambda^n F(\boldsymbol{V}) \quad \forall \boldsymbol{V} \in \mathcal{W}_0,$$

where $A_{\boldsymbol{up}\boldsymbol{S}'\varphi}(\boldsymbol{V}, \boldsymbol{U})$ is a semilinear form defined on $\mathcal{W}_0 \times \mathcal{W}$ as

$$\begin{aligned} A_{\boldsymbol{up}\boldsymbol{S}'\varphi}(\boldsymbol{V}, \boldsymbol{U}) := {} & \langle \boldsymbol{\nabla}_0 \boldsymbol{v}, \boldsymbol{F} \cdot \boldsymbol{S}_{em} \rangle + \left\langle \boldsymbol{\nabla}_0 \boldsymbol{v}, \boldsymbol{F} \cdot \boldsymbol{S}' \right\rangle - \left\langle \boldsymbol{\nabla}_0 \boldsymbol{v}, pJ\boldsymbol{F}^{-\mathrm{T}} \right\rangle + \left\langle q, \frac{d\hat{\Psi}^{vol}_m}{dJ} \right\rangle + \left\langle q, \frac{p}{\kappa} \right\rangle - \left\langle \boldsymbol{T}, 2\frac{\partial \Psi'_m}{\partial \boldsymbol{C}} \right\rangle \\ & + \left\langle \boldsymbol{T}, \boldsymbol{S}' \right\rangle - \langle \boldsymbol{\nabla}_0 \eta, \boldsymbol{D}_0 \rangle, \end{aligned}$$

and $F(\boldsymbol{V})$ is the same linear form defined in Equation (23).

4.2.3 | Linearization

After using a Newton-Raphson scheme, we obtain the following linearized form of the problem. Given $\boldsymbol{U}$ as the guess for the solution at the previous iteration and at load increment n, find a correction $\boldsymbol{\delta U} := \left[\boldsymbol{\delta u}, \delta p, \boldsymbol{\delta S'}, \delta\varphi\right]^T \in \mathcal{W}_0$ such that

$$B_{upS'\varphi}(\boldsymbol{U}; \boldsymbol{V}, \boldsymbol{\delta U}) = \lambda^n F(\boldsymbol{V}) - A_{upS'\varphi}(\boldsymbol{V}, \boldsymbol{U}) \quad \forall \boldsymbol{V} \in \mathcal{W}_0 \tag{30}$$

where $B_{upS'\varphi}(\boldsymbol{U}; \boldsymbol{V}, \boldsymbol{\delta U})$ is the bilinear form obtained through the Newton-Raphson linearization, and it is defined on $\mathcal{W}_0 \times \mathcal{W}_0$ as

$$\begin{aligned} B_{upS'\varphi}(\boldsymbol{U}; \boldsymbol{V}, \boldsymbol{\delta U}) \; :=\; & \langle \boldsymbol{\nabla}_0 \boldsymbol{v}, \boldsymbol{\nabla}_0 \boldsymbol{\delta u} \cdot \boldsymbol{S}_{em} \rangle + \left\langle \boldsymbol{F}^T \cdot \boldsymbol{\nabla}_0 \boldsymbol{v}, \mathbb{C}_{em} : \left(\boldsymbol{F}^T \cdot \boldsymbol{\nabla}_0 \boldsymbol{\delta u} \right) \right\rangle + \left\langle \boldsymbol{F}^T \cdot \boldsymbol{\nabla}_0 \boldsymbol{v}, \mathbb{P}_{em} \cdot \boldsymbol{\nabla}_0 \delta\varphi \right\rangle + \left\langle \boldsymbol{\nabla}_0 \boldsymbol{v}, \boldsymbol{\nabla}_0 \boldsymbol{\delta u} \cdot \boldsymbol{S'} \right\rangle \\ & + \left\langle \boldsymbol{\nabla}_0 \boldsymbol{v}, \boldsymbol{F} \cdot \boldsymbol{\delta S'} \right\rangle - \left\langle \boldsymbol{\nabla}_0 \boldsymbol{v}, J p\left(\boldsymbol{\nabla}_0 \boldsymbol{\delta u} : \boldsymbol{F}^{-1} \right) \boldsymbol{F}^{-T} \right\rangle + \left\langle \boldsymbol{\nabla}_0 \boldsymbol{v}, J p\left(\boldsymbol{F}^{-1} \cdot \boldsymbol{\nabla}_0 \boldsymbol{\delta u} \cdot \boldsymbol{F}^{-1} \right)^T \right\rangle \\ & - \left\langle \boldsymbol{\nabla}_0 \boldsymbol{v}, \delta p J \boldsymbol{F}^{-\mathrm{T}} \right\rangle + \left\langle q, J \frac{d^2 \hat{\Psi}^{vol}_m}{d J^2} \boldsymbol{\nabla}_0 \boldsymbol{\delta u} : \boldsymbol{F}^{-T} \right\rangle + \left\langle q, \frac{\delta p}{\kappa} \right\rangle - \left\langle \boldsymbol{T}, \mathbb{C}' : \left(\boldsymbol{F}^T \cdot \boldsymbol{\nabla}_0 \boldsymbol{\delta u} \right) \right\rangle \\ & + \left\langle \boldsymbol{T}, \boldsymbol{\delta S'} \right\rangle - \left\langle \boldsymbol{\nabla}_0 \eta, \mathbb{P}_{em} : \left(\boldsymbol{F}^T \cdot \boldsymbol{\nabla}_0 \boldsymbol{\delta u} \right) \right\rangle + \langle \boldsymbol{\nabla}_0 \eta, \mathbb{E}_{em} \cdot \boldsymbol{\nabla}_0 \delta\varphi \rangle. \end{aligned}$$

Now $\boldsymbol{S}_{em}$, $\boldsymbol{F}$, J and the constitutive tensors are evaluated with the given guess $\boldsymbol{U}$, but $\boldsymbol{S'}$ is an independent variable.

4.2.4 | Symmetrization

The symmetric form of the problem can be defined as

$$B^{\,sym}_{upS'\varphi}(\boldsymbol{U}; \boldsymbol{V}, \boldsymbol{\delta U}) = \lambda^n F(\boldsymbol{V}) - A^{\mathrm{sym}}_{upS'\varphi}(\boldsymbol{V}, \boldsymbol{U}) \quad \forall \boldsymbol{V} \in \mathcal{W}_0, \tag{31}$$

where

$$\begin{aligned} B^{\mathrm{sym}}_{upS'\varphi}(\boldsymbol{U}; \boldsymbol{V}, \boldsymbol{\delta U}) :=\; & \langle \boldsymbol{\nabla}_0 \boldsymbol{v}, \boldsymbol{\nabla}_0 \boldsymbol{\delta u} \cdot \boldsymbol{S}_{em} \rangle + \left\langle \boldsymbol{F}^T \cdot \boldsymbol{\nabla}_0 \boldsymbol{v}, \mathbb{C}_{em} : \left(\boldsymbol{F}^T \cdot \boldsymbol{\nabla}_0 \boldsymbol{\delta u} \right) \right\rangle \\ & + \left\langle \boldsymbol{F}^T \cdot \boldsymbol{\nabla}_0 \boldsymbol{v}, \mathbb{P}_{em} \cdot \boldsymbol{\nabla}_0 \delta\varphi \right\rangle + \left\langle \boldsymbol{\nabla}_0 \boldsymbol{v}, \boldsymbol{\nabla}_0 \boldsymbol{\delta u} \cdot \boldsymbol{S'} \right\rangle + \left\langle \boldsymbol{\nabla}_0 \boldsymbol{v}, \boldsymbol{F} \cdot \boldsymbol{\delta S'} \right\rangle \\ & - \left\langle \boldsymbol{\nabla}_0 \boldsymbol{v}, J p\left(\boldsymbol{\nabla}_0 \boldsymbol{\delta u} : \boldsymbol{F}^{-1} \right) \boldsymbol{F}^{-T} \right\rangle + \left\langle \boldsymbol{\nabla}_0 \boldsymbol{v}, J p\left(\boldsymbol{F}^{-1} \cdot \boldsymbol{\nabla}_0 \boldsymbol{\delta u} \cdot \boldsymbol{F}^{-1} \right)^T \right\rangle \\ & - \left\langle \boldsymbol{\nabla}_0 \boldsymbol{v}, \delta p J \boldsymbol{F}^{-\mathrm{T}} \right\rangle + \left\langle q, J \boldsymbol{\nabla}_0 \boldsymbol{\delta u} : \boldsymbol{F}^{-T} \right\rangle + \left\langle q, \left(\frac{d^2 G}{d J^2} \right)^{-1} \frac{\delta p}{\kappa} \right\rangle \\ & - \langle \boldsymbol{T}, \boldsymbol{F} \cdot \boldsymbol{\nabla}_0 \boldsymbol{\delta u} \rangle + \left\langle \boldsymbol{T}, \mathbb{D}' : \boldsymbol{\delta S'} \right\rangle \\ & - \left\langle \boldsymbol{\nabla}_0 \eta, \mathbb{P}_{em} : \left(\boldsymbol{F}^T \cdot \boldsymbol{\nabla}_0 \boldsymbol{\delta u} \right) \right\rangle + \langle \boldsymbol{\nabla}_0 \eta, \mathbb{E}_{em} \cdot \boldsymbol{\nabla}_0 \delta\varphi \rangle. \\ A^{\mathrm{sym}}_{upS'\varphi}(\boldsymbol{V}, \boldsymbol{U}) :=\; & \langle \boldsymbol{\nabla}_0 \boldsymbol{v}, \boldsymbol{F} \cdot \boldsymbol{S}_{em} \rangle + \left\langle \boldsymbol{\nabla}_0 \boldsymbol{v}, \boldsymbol{F} \cdot \boldsymbol{S'} \right\rangle - \left\langle \boldsymbol{\nabla}_0 \boldsymbol{v}, p J \boldsymbol{F}^{-\mathrm{T}} \right\rangle \\ & + \left\langle q, \left(\frac{d^2 G}{d J^2} \right)^{-1} \frac{d G}{d J} \right\rangle + \left\langle q, \left(\frac{d^2 G}{d J^2} \right)^{-1} \frac{p}{\kappa} \right\rangle - \left\langle \boldsymbol{T}, \mathbb{D}' : 2 \frac{\partial \Psi'_m}{\partial \boldsymbol{C}} \right\rangle \\ & + \left\langle \boldsymbol{T}, \mathbb{D}' : \boldsymbol{S'} \right\rangle - \langle \boldsymbol{\nabla}_0 \eta, \boldsymbol{D}_0 \rangle. \end{aligned}$$

It is important to note that the second equation has been multiplied by the linearized term $\left(\frac{d^2 \hat{\Psi}^{vol}_m}{d J^2} \right)^{-1}$, and the third equation by $\mathbb{D}'$, the deviatoric part of the flexibility tensor. Defining this fourth-order tensor requires obtaining the inverse strain energy function, which entails solving a nonlinear problem. For simplicity, we will use the non-symmetric form of the problem in the following analysis, although employing the symmetric version would be straightforward.

4.2.5 | Galerkin Spatial Discretization

The Galerkin discrete version of problem (30) is: For a given load increment λ^n and a fixed iteration, find $\boldsymbol{\delta U}_h := \left[\boldsymbol{\delta u}_h, \delta p_h, \boldsymbol{\delta S}'_h, \delta\varphi_h\right]^T \in \mathcal{W}_{h,0}$ such that

$$B_{\boldsymbol{upS}'\varphi}\left(\boldsymbol{U}_h; \boldsymbol{V}_h, \boldsymbol{\delta U}_h\right) = \lambda^n F\left(\boldsymbol{V}_h\right) - A_{\boldsymbol{upS}'\varphi}\left(\boldsymbol{V}_h, \boldsymbol{U}_h\right) \quad \forall \boldsymbol{V}_h \in \mathcal{W}_{h,0}.$$

As before, the stability of the discrete formulation relies on compatibility restrictions between the interpolation functions selected for the displacement, pressure, deviatoric PK2 mechanical stress, and electric potential fields, as dictated by the appropriate inf-sup condition [63]. To address the instabilities discussed earlier, we propose the stabilization technique outlined in Section 2.5.

Remark 4.3. As for previous problems, let us consider the symmetrized problem (31) and discuss the stability of this linearized problem. Taking $\boldsymbol{v}_h = \boldsymbol{\delta u}_h$, $\eta_h = \delta\varphi_h$ (assuming homogeneous Dirichlet boundary conditions), $q_h = \delta p_h$ and $\boldsymbol{T}_h = \boldsymbol{\delta S}'_h$ it is found that

$$\begin{aligned} B^{\text{sym}}_{\boldsymbol{upS}'\varphi}\left(\boldsymbol{U}_h; \boldsymbol{\delta U}_h, \boldsymbol{\delta U}_h\right) :=& \left\langle \boldsymbol{\nabla}_0 \boldsymbol{\delta u}_h, \boldsymbol{\nabla}_0 \boldsymbol{\delta u}_h \cdot \boldsymbol{S}_{em} \right\rangle + \left\langle \boldsymbol{F}^T \cdot \boldsymbol{\nabla}_0 \boldsymbol{\delta u}_h, \mathbb{C}_{em} : \left(\boldsymbol{F}^T \cdot \boldsymbol{\nabla}_0 \boldsymbol{\delta u}_h\right) \right\rangle + \left\langle \boldsymbol{\nabla}_0 \boldsymbol{\delta u}_h, \boldsymbol{\nabla}_0 \boldsymbol{\delta u}_h \cdot \boldsymbol{S}' \right\rangle \\ &- \left\langle \boldsymbol{\nabla}_0 \boldsymbol{\delta u}_h, J p_h \left(\boldsymbol{\nabla}_0 \boldsymbol{\delta u}_h : \boldsymbol{F}^{-1}\right) \boldsymbol{F}^{-T} \right\rangle + \left\langle \boldsymbol{\nabla}_0 \boldsymbol{\delta u}_h, J p_h \left(\boldsymbol{F}^{-1} \cdot \boldsymbol{\nabla}_0 \boldsymbol{\delta u}_h \cdot \boldsymbol{F}^{-1}\right)^T \right\rangle \\ &+ \left\langle \delta p_h, \left(\frac{d^2 \hat{\Psi}^{vol}_m}{d J^2} \right)^{-1} \frac{\delta p_h}{\kappa} \right\rangle + \left\langle \boldsymbol{\delta S}'_h, \mathbb{D}' : \boldsymbol{\delta S}'_h \right\rangle + \left\langle \boldsymbol{\nabla}_0 \delta\varphi_h, \mathbb{E}_{em} \cdot \boldsymbol{\nabla}_0 \delta\varphi_h \right\rangle. \end{aligned}$$

In this case, we have the same control over the increment of the electric potential field as in the $\boldsymbol{up\varphi}$ formulation due to the second-order dielectric tensor $\mathbb{E}_{em}$. However, there is no term that guarantees stability for the displacement increment, as none of them involve matrices that are required to be positive definite. Consequently, control over the displacement increment cannot be ensured. Additionally, the flexibility matrix is a positive-definite tensor, which provides control over the increment of the deviatoric PK2 stress, $\boldsymbol{\delta S}'_h$. It is again evident that in the nearly and fully incompressible cases, as $\kappa \to \infty$, the increment of pressure δp_h becomes uncontrollable.

Therefore, the Galerkin formulation is only stable if two inf-sup conditions are satisfied, one between the displacements and the deviatoric PK2 mechanical stresses and another one between the displacements and the pressure. These conditions are explained in [54] for the linear Stokes problem, and are obviously inherited in the nonlinear problem considered now. Only deviatoric PK2 mechanical stresses can be controlled with the Galerkin formulation, and in the case of compressible materials, also the pressure, but this control disappears as $\kappa \to \infty$. Displacement gradients need to be controlled using an inf-sup condition, and pressures (regardless of the compressibility) using another one. The alternative to using the Galerkin method with FE spaces satisfying the inf-sup conditions is to use a stabilized FE method, as the one we describe next.

4.2.6 | Stabilized Formulation

According to the VMS framework explained in Section 2.5, the stabilized problem with S-OSGS is defined as

$$\begin{aligned} &B_{\boldsymbol{upS}'\varphi}\left(\boldsymbol{U}_h; \boldsymbol{V}_h, \boldsymbol{\delta U}_h\right) + \sum_K \left\langle \hat{\mathscr{L}}^*_{\boldsymbol{upS}'\varphi}(\boldsymbol{U}_h; \boldsymbol{V}_h), \boldsymbol{\tau}_K \tilde{\Pi}\left[\lambda^n \, f - \hat{\mathscr{A}}_{\boldsymbol{upS}'\varphi}(\boldsymbol{U}_h) - \hat{\mathscr{L}}_{\boldsymbol{upS}'\varphi}(\boldsymbol{U}_h; \boldsymbol{\delta U}_h)\right] \right\rangle_K \\ &\qquad = \lambda^n F\left(\boldsymbol{V}_h\right) - A_{\boldsymbol{upS}'\varphi}\left(\boldsymbol{V}_h, \boldsymbol{U}_h\right) \quad \forall \boldsymbol{V}_h \in \mathcal{W}_{h,0}. \end{aligned}$$

As in previous problems, $\boldsymbol{\tau}_K$ is taken again as a diagonal matrix of stabilization parameters, $\boldsymbol{\tau}_K = \text{diag}\left(\tau_{\boldsymbol{u}} \boldsymbol{I}_d, 0, \tau_{\boldsymbol{S}'} \boldsymbol{I}_{d\times d},\right)$, with $\boldsymbol{I}_{d\times d}$ the identity on second-order tensors and parameters $\tau_{\boldsymbol{u}}$ and $\tau_{\boldsymbol{S}'}$ are again coefficients coming from the study of the behavior of the stabilization parameters based on a Fourier analysis of the problem for the SGSs. In this case, we propose to use the stabilization parameters presented in [59] for finite strain solid mechanics problems

$$\tau_{\boldsymbol{u}} = c_2 \frac{h_K^2}{2\mu} \quad \text{and} \quad \tau_{\boldsymbol{S}'} = c_3, \tag{32}$$

where c_2 and c_3 are algorithmic parameters which must be determined. The split operators we need to define to have control over both the displacement and the pressure field are

$$\hat{\mathscr{A}}_{upS'\varphi}(\boldsymbol{U}) = \begin{bmatrix} \boldsymbol{\nabla}_0 \cdot \{pJ\boldsymbol{F}^{-\mathrm{T}}\} \\ 0 \\ -2\frac{\partial \Psi'_m}{\partial \boldsymbol{C}} \end{bmatrix}, \quad \hat{\mathscr{L}}^*_{upS'\varphi}(\boldsymbol{U};\boldsymbol{V}) = \begin{bmatrix} -\boldsymbol{\nabla}_0 \cdot \left\{ qJ\frac{d^2\hat{\Psi}^{vol}_m}{dJ^2}\boldsymbol{F}^{-\mathrm{T}} \right\} \\ 0 \\ \boldsymbol{F}^T \cdot \boldsymbol{\nabla}_0 \boldsymbol{v} \end{bmatrix},$$

$$\hat{\mathscr{L}}_{upS'\varphi}(\boldsymbol{U};\delta\boldsymbol{U}) = \begin{bmatrix} \boldsymbol{\nabla}_0 \cdot \left\{ -Jp\left(\boldsymbol{\nabla}_0\delta\boldsymbol{u} : \boldsymbol{F}^{-1}\right)\boldsymbol{F}^{-T} + Jp\left(\boldsymbol{F}^{-1}\cdot\boldsymbol{\nabla}_0\delta\boldsymbol{u}\cdot\boldsymbol{F}^{-1}\right)^T + \delta pJ\boldsymbol{F}^{-\mathrm{T}} \right\} \\ 0 \\ -\mathbb{C}' : \left(\boldsymbol{F}^T \cdot \boldsymbol{\nabla}_0\delta\boldsymbol{u}\right) \end{bmatrix}.$$

Thus, we introduce the term $\sum_K \tau_{\boldsymbol{u}} \left\langle \boldsymbol{\nabla}_0 \cdot \left\{ qJ\frac{d^2\hat{\Psi}^{vol}_m}{dJ^2}\boldsymbol{F}^{-\mathrm{T}} \right\}, \tilde{\Pi}\left[\boldsymbol{\nabla}_0 \cdot \{\delta pJ\boldsymbol{F}^{-\mathrm{T}}\}\right] \right\rangle_K$ on the left-hand side of the system, which provides control over the pressure gradient. Furthermore, the term $\sum_K \tau_{S'} \left\langle \boldsymbol{F}^T \cdot \boldsymbol{\nabla}_0\boldsymbol{v}, \tilde{\Pi}\left[-\mathbb{C}' : \left(\boldsymbol{F}^T \cdot \boldsymbol{\nabla}_0\delta\boldsymbol{u}\right)\right] \right\rangle_K$ allows us to control the displacement gradient thanks to the fact that $\mathbb{C}'$ is a positive-definite tensor. The control on the deviatoric PK2 stresses provided by the Galerkin terms is enough if a continuous stress interpolation is adopted. Nevertheless, if this interpolation is discontinuous, additional terms involving jumps across inter-element boundaries of the normal component of the stresses may need to be added. When discontinuous pressures are used, these terms can be derived from SGSs on the element boundaries. See [65] for a heuristic motivation and [54] for the analysis in a linearized problem.

5 | Block-Iterative Scheme

The objective of this work is to approximate a coupled system in which the coupling comes from different physical phenomena. Numerical methods applied to these coupled problems lead to the solution of a set of nonlinear algebraic equations. The discretization of the entire set of governing equations in finite strain electromechanics presented in system (20) leads to a nonlinear algebraic system of equations of the form:

$$\begin{aligned} \boldsymbol{A}_{\boldsymbol{D}}(\boldsymbol{D},\boldsymbol{\varphi}) &= \boldsymbol{f}_{\boldsymbol{D}}, \\ \boldsymbol{A}_{\boldsymbol{\varphi}}(\boldsymbol{D},\boldsymbol{\varphi}) &= \boldsymbol{f}_{\boldsymbol{\varphi}}, \end{aligned} \tag{33}$$

where $\boldsymbol{D}$ is the vector of unknowns of the mechanical field, which depends upon the selected formulation, containing the nodal unknowns of $[\boldsymbol{u}, p]^T$ for the mixed $\boldsymbol{u}p\boldsymbol{\varphi}$ formulation and of $\left[\boldsymbol{u}, p, \boldsymbol{S}'\right]^T$ for the mixed $\boldsymbol{u}p\boldsymbol{S}'\boldsymbol{\varphi}$ formulation. $\boldsymbol{\varphi}$ is the vector of unknowns of the electric problem, which in this case only considers the electric potential field, φ. Furthermore, $\boldsymbol{f}_{\boldsymbol{D}}$ and $\boldsymbol{f}_{\boldsymbol{\varphi}}$ are the vectors of "force" terms. Thus, the alternatives to solve the coupled problem are twofold and are described below.

Monolithic strategy. When the nonlinear equations in system (33) are treated simultaneously, this leads to the monolithic scheme of the problem. This strategy necessarily requires the development of a special-purpose code. The scalability and computational cost can become expensive as the number of variables and equations increases. It presents less modularity in parallelization compared to the staggered strategy presented below. Also, in general, these variables will not be homogeneous, as they arise from the discretization of different physical phenomena. The solution to this nonlinear problem for a given value of the load factor λ^n can be obtained by making use of a Newton-Raphson iteration scheme according to

$$\begin{bmatrix} \boldsymbol{B}_{\boldsymbol{D}\boldsymbol{D}}(\boldsymbol{D}^i,\boldsymbol{\varphi}^i) & \boldsymbol{B}_{\boldsymbol{D}\boldsymbol{\varphi}}(\boldsymbol{D}^i,\boldsymbol{\varphi}^i) \\ \boldsymbol{B}_{\boldsymbol{\varphi}\boldsymbol{D}}(\boldsymbol{D}^i,\boldsymbol{\varphi}^i) & \boldsymbol{B}_{\boldsymbol{\varphi}\boldsymbol{\varphi}}(\boldsymbol{D}^i,\boldsymbol{\varphi}^i) \end{bmatrix} \begin{bmatrix} \delta\boldsymbol{D}^{i+1} \\ \delta\boldsymbol{\varphi}^{i+1} \end{bmatrix} = \lambda^n \begin{bmatrix} \boldsymbol{f}_{\boldsymbol{D}} \\ \boldsymbol{f}_{\boldsymbol{\varphi}} \end{bmatrix} - \begin{bmatrix} \boldsymbol{A}_{\boldsymbol{D}}(\boldsymbol{D}^i,\boldsymbol{\varphi}^i) \\ \boldsymbol{A}_{\boldsymbol{\varphi}}(\boldsymbol{D}^i,\boldsymbol{\varphi}^i) \end{bmatrix}, \tag{34}$$

where $\{\boldsymbol{D}^i, \boldsymbol{\varphi}^i\}$ represents the value of fields $\{\boldsymbol{D}, \boldsymbol{\varphi}\}$ at the Newton-Raphson iteration i (and load step n, which is omitted to lighten the notation) and the four-block (stiffness) matrix on the left-hand side stems from the linearization of system (33) with respect to increments $\{\delta\boldsymbol{D}^{i+1}, \delta\boldsymbol{\varphi}^{i+1}\}$. The latter permits to update the values of $\{\boldsymbol{D}, \boldsymbol{\varphi}\}$ according to

$$\boldsymbol{D}^{i+1} = \boldsymbol{D}^i + \delta\boldsymbol{D}^{i+1}, \qquad \boldsymbol{\varphi}^{i+1} = \boldsymbol{\varphi}^i + \delta\boldsymbol{\varphi}^{i+1}.$$

Staggered strategy. The second alternative is to treat each problem one at a time, considering the coupling terms as forcing terms on the right-hand side of the equations. This leads to several sets of algebraic equations, each of them to be solved solely for the variables related to one problem [61]. Let us consider now the use of block-iterative algorithms to solve problem (33). This will reduce the size of the resulting subproblems at the expense of iterating.

To begin, we must first focus on the conservation of linear momentum presented in Equation (20a). In this case, the term that introduces coupling between variables is the electromechanical stress tensor $\boldsymbol{S}_{em}\left(\boldsymbol{u}^{k+1}, \boldsymbol{\varphi}^{k+1}\right)$. Here, superscript k refers to the coupling iteration counter within a load step n (again, omitted). The main idea to develop the block-iterative scheme involves approximating the dependence of the stresses $\boldsymbol{S}_{em}$ on the electric potential field from the previous coupling, such that $\boldsymbol{S}_{em}\left(\boldsymbol{u}^{k+1}, \boldsymbol{\varphi}^{k+1}\right) \approx \boldsymbol{S}_{em}\left(\boldsymbol{u}^{k+1}, \boldsymbol{\varphi}^{k}\right)$. Once this approximation is applied, we can omit the linearization matrix $\boldsymbol{B}_{\boldsymbol{D}\boldsymbol{\varphi}}$, as the electric potential for this coupling iteration is considered known. From the first row of the system (34), we can derive a linear system of equations to obtain the increment $\boldsymbol{\delta D}$. Therefore, at load increment n, coupling iteration $k+1$ and nonlinear iteration $i+1$, the first system of equations to be solved is

$$\boldsymbol{B}_{\boldsymbol{D}\boldsymbol{D}}(\boldsymbol{D}^{i}, \boldsymbol{\varphi}^{k})\boldsymbol{\delta D}^{i+1} = \lambda^{n}\boldsymbol{f}_{\boldsymbol{D}} - \boldsymbol{A}_{\boldsymbol{D}}(\boldsymbol{D}^{i}, \boldsymbol{\varphi}^{k}), \tag{35a}$$

$$\boldsymbol{D}^{i+1} = \boldsymbol{D}^{i} + \boldsymbol{\delta D}^{i+1}. \tag{35b}$$

Note that the complete set of superscripts for $\boldsymbol{D}^{i+1}$ is $\boldsymbol{D}^{n,k+1,i+1}$. Once we solve the nonlinear iterations and achieve convergence (measured with some fixed tolerance tol, $||\boldsymbol{D}^{i+1} - \boldsymbol{D}^{i}|| \leq \text{tol}$), we obtain $\boldsymbol{D}^{k+1} = \boldsymbol{D}^{i+1}$, the value for the mechanical unknowns for the current coupling iteration. With this value, we can proceed to the second row of the system (34). In this case, since $\boldsymbol{D}^{k+1}$ is now known, the term $\boldsymbol{B}_{\boldsymbol{\varphi}\boldsymbol{D}}$ must be omitted from the linearization. This allows us to formulate a second system of equations to obtain the increment of the electric potential $\boldsymbol{\delta\varphi}$. Therefore, at load increment n, coupling iteration $k+1$ and nonlinear iteration $i+1$, the second system of equations to be solved is

$$\boldsymbol{B}_{\boldsymbol{\varphi}\boldsymbol{\varphi}}(\boldsymbol{D}^{k+1}, \boldsymbol{\varphi}^{i})\boldsymbol{\delta\varphi}^{i+1} = \lambda^{n}\boldsymbol{f}_{\boldsymbol{\varphi}} - \boldsymbol{A}_{\boldsymbol{\varphi}}(\boldsymbol{D}^{k+1}, \boldsymbol{\varphi}^{i}), \tag{36a}$$

$$\boldsymbol{\varphi}^{i+1} = \boldsymbol{\varphi}^{i} + \boldsymbol{\delta\varphi}^{i+1}. \tag{36b}$$

Again, once we solve the nonlinear iterations and achieve convergence (measured with some fixed tolerance tol, $||\boldsymbol{\varphi}^{i+1} - \boldsymbol{\varphi}^{i}|| \leq \text{tol}$), we obtain $\boldsymbol{\varphi}^{k+1} = \boldsymbol{\varphi}^{i+1}$, the value for the electric potential unknown for the current coupling iteration.

This procedure must be repeated until the values between coupling iterations converge, also measured with a given tolerance. Once convergence is achieved, the next load factor can be taken, and the process repeated. This method is the one considered in all the numerical examples developed in this work.

The staggered approach may be beneficial for this type of coupled problem. On one hand, the convex/concave nature of the free energy density (at least near the origin) yields a saddle point problem [30]. On the other hand, the mechanical and electrical properties may differ by several orders of magnitude, although appropriate scaling can help mitigate this issue [75]. These factors can complicate the use of iterative solvers for the monolithic approach, particularly in computationally intensive problems. Additionally, by solving the mechanical and electrical problems separately, the staggered approach is often less intrusive and more easily integrated into in-house computational platforms.

To conclude this section, Algorithm 1 presents the staggered approach employed in this work. Let us also note that the coupling and linearization loops could be collapsed into a single loop instead of using nested loops. This would amount to replace $\boldsymbol{\varphi}^{k}$ by $\boldsymbol{\varphi}^{i}$ in Equation (35a) and $\boldsymbol{D}^{k+1}$ by $\boldsymbol{D}^{i+1}$ in Equation (36a). In this case, convergence would be, at most, linear.

6 | Numerical Examples

In this section, a series of numerical examples for electromechanics are presented to assess the performance, robustness, accuracy, and applicability of the proposed stabilized mixed formulations. As a first case, a test with a manufactured solution is considered to analyze the spatial discretization errors upon mesh refinement for both formulations presented in this work. The second example we aim to study involves the bending of a beam induced by the application of an electric field. The objective of this example is to analyze and examine the shear-locking behavior that our formulations may exhibit as the beams become more slender, and thus determine the range of applicability of each formulation. Finally, two 3D cases will be studied and carried out for the two formulations presented in this work, to further analyze the drawbacks and advantages of each one.

ALGORITHM 1 | Block-iterative scheme to solve the nonlinear electromechanics problem.

- $n = 0$; loop over the number of load increments, N.

  Initialize $\boldsymbol{\varphi}^{n=0} = \mathbf{0}$, $\boldsymbol{D}^{n=0} = \mathbf{0}$.

  $n \leftarrow n + 1$, $\lambda^n = n/N$.

  Initialize $\boldsymbol{\varphi}^{n,k=0} \equiv \boldsymbol{\varphi}^0 \leftarrow \boldsymbol{\varphi}^{n-1}$, $\boldsymbol{D}^{n,k=0} \equiv \boldsymbol{D}^0 \leftarrow \boldsymbol{D}^{n-1}$.
  - $k = 0$; coupling loop, iterate until convergence.
    - **Solve the equations for the solid solver**, using $\boldsymbol{\varphi}^k$ for $\boldsymbol{\varphi}$. At the load increment n, omitting the superscript $k + 1$ for the unknowns, these equations are:

$$
\begin{aligned}
-\boldsymbol{\nabla}_0 \cdot \{\boldsymbol{F} \cdot \boldsymbol{S}_{em}\} - \boldsymbol{\nabla}_0 \cdot \{\boldsymbol{F} \cdot \boldsymbol{S}'\} + \boldsymbol{\nabla}_0 \cdot \{pJ\boldsymbol{F}^{-\mathrm{T}}\} &= \lambda^n \boldsymbol{f}_0 && \text{in } V,\\
\frac{p}{\kappa} + \frac{d\hat{\Psi}_{\mathrm{m}}^{\mathrm{vol}}}{dJ} &= 0 && \text{in } V,\\
\boldsymbol{S}' - 2\frac{\partial \Psi'_m}{\partial \boldsymbol{C}} &= \mathbf{0} && \text{in } V,\\
\{\boldsymbol{F} \cdot \boldsymbol{S}_{em} + \boldsymbol{F} \cdot \boldsymbol{S}' - pJ\boldsymbol{F}^{-\mathrm{T}}\} \cdot \boldsymbol{N} &= \lambda^n \boldsymbol{t}_0 && \text{on } \partial V_{\mathrm{t}},\\
\boldsymbol{u} &= \boldsymbol{u}_{\mathrm{D}} && \text{on } \partial V_{\mathrm{u}}.
\end{aligned}
$$

    - Once converged, **update the value for the mechanical unknowns** $\boldsymbol{D}^{k+1}$ depending on the selected formulation described in Section 4.
    - **Solve the equations for the electrostatics solver**, using $\boldsymbol{D}^{k+1}$ for $\boldsymbol{D}$. At the load increment λ^n, omitting the superscript $k + 1$ for the unknowns, these equations are:

$$
\begin{aligned}
\boldsymbol{\nabla}_0 \cdot \boldsymbol{D}_0 &= \lambda^n \rho_0^{\mathrm{e}} && \text{in } V,\\
\boldsymbol{E}_0 + \boldsymbol{\nabla}_0 \varphi &= \mathbf{0} && \text{in } V,\\
\boldsymbol{D}_0 + \frac{\partial \Psi_{em}}{\partial \boldsymbol{E}_0} &= \mathbf{0} && \text{in } V,\\
\boldsymbol{D}_0 \cdot \boldsymbol{N} &= -\lambda^n \omega_0^{\mathrm{e}} && \text{on } \partial V_{\omega},\\
\varphi &= \varphi_{\mathrm{D}} && \text{on } \partial V_{\varphi}.
\end{aligned}
$$

    - Once converged, **update the value for the electric unknowns** $\boldsymbol{\varphi}^{k+1}$.
    - **Check convergence and update unknowns** for the next coupling iteration. When coupling conditions are satisfied up to a tolerance, the coupling iterative loop ends.
      $k \leftarrow k + 1$.

  End block-iterative loop.

  End loop over the number of load increments.

Concerning the block-iterative scheme, for all examples, a maximum of 10 iterations is set for both the solid and the electric sub-problems, whose numerical relative tolerance in the $L^2(V)$ norm is 10^{-5} unless specified. Also, for the coupling conditions, the relative tolerance is 10^{-3}. To solve the monolithic system of linear equations for each sub-problem, we consider direct solvers, which are implemented in the `PETSc` parallel solver library [76].

For all the numerical examples included next, hyperelastic models are considered fully incompressible, and so the bulk modulus is $\kappa = \infty$ and the Poisson ratio $\nu = 0.5$, unless otherwise specified. The algorithmic parameters c_1, c_2, and c_3 are determined in the first numerical example and fixed for the rest of the study. As previously discussed, the nonlinearities in the problem are solved via a Newton-Raphson scheme. Depending on the nonlinearities, the initial guess of the iterative procedure needs to be close enough to the solution to guarantee convergence of the nonlinear iterations. In our case, the load increment is the parameter that controls the evolution of the nonlinear iterations, so we will have to tune it depending on the nonlinearities of each numerical example. Unless otherwise stated, all numerical examples are conducted using 10 load increments.

In the $\boldsymbol{upS'\varphi}$ formulation, we ensure the symmetry of the deviatoric component of the PK2 stress by explicitly imposing this condition through the use of Voigt's notation. This approach allows us to represent the deviatoric stress tensor as a vector with three components in 2D and six components in 3D. As a result, the symmetry condition is inherently satisfied within the formulation. Let us note that this can be done because of the stabilized formulation we use, since in some cases, using the Galerkin method, symmetry can only be imposed weakly when stresses are introduced as unknowns (see, e.g., [77]).

To ensure a fair comparison between the different formulations, we will compare the results with respect to the number of Degrees Of Freedom (DOFs) in the whole algebraic system.

6.1 | A Test With Analytical Solution

Let us first perform a simple test whose main objective is to numerically check the order of convergence of the proposed scheme with respect to the mesh size. This problem will allow us to tune the optimal stabilization coefficients. For this purpose, we use the so-called method of manufactured solutions.

In this procedure, an exact analytical solution is defined a priori and later substituted into the continuum equations to obtain associated forcing terms. These forcing terms are then introduced as perturbations in the FE computation. The manufactured solutions are composed of smooth functions. Dirichlet boundary conditions are prescribed over the boundaries upon evaluation of the displacement and electric potential analytical solutions.

The region we consider is the unit square plate $V = [0,1] \times [0,1]$ under plain strain assumption, and we impose the following manufactured displacement, pressure, and electric potential fields

$$\begin{aligned} \boldsymbol{u}(X,Y) &= k[\exp(X+Y), -\exp(X+Y)], \\ p(X,Y) &= \mu \sin(2\pi X)\sin(2\pi Y), \\ \varphi(X,Y) &= k \sin(2\pi X)\sin(2\pi Y). \end{aligned}$$

where $k = 0.01$ and X and Y referring to the Cartesian axes in the reference configuration. All quantities are assumed dimensionless in this example. It is important to note that this displacement field gives an incompressible motion due to the fact that the Jacobian $J(\boldsymbol{u}(X,Y)) = 1$ for all X, Y. We set a Neo-Hookean (see Equation (12)) material for the deviatoric part of the stresses, with shear modulus $\mu = \frac{10^7}{3}$ and Poisson ratio $\nu = 0.5$ and a quadratic law for the volumetric response (see Equation (14)). The material is selected to be an ideal isotropic dielectric elastomer (see Equation (9)), being the electric permittivity of the dielectric $\varepsilon = 1$. Therefore, the manufactured deviatoric PK2 mechanical stress is computed with respect to the manufactured displacement field as

$$\boldsymbol{S'}(X,Y) = \mu\left\{\boldsymbol{I} - \frac{1}{3}\text{trace}[\boldsymbol{C}(\boldsymbol{u}(X,Y))]\boldsymbol{C}^{-1}(\boldsymbol{u}(X,Y))\right\}.$$

We study the convergence behavior of the proposed method by running the case on seven meshes obtained by refinement. The sequence is of structured grids of n^2 linear and quadratic quadrilateral elements, being n the number of FEs along each side of the domain.

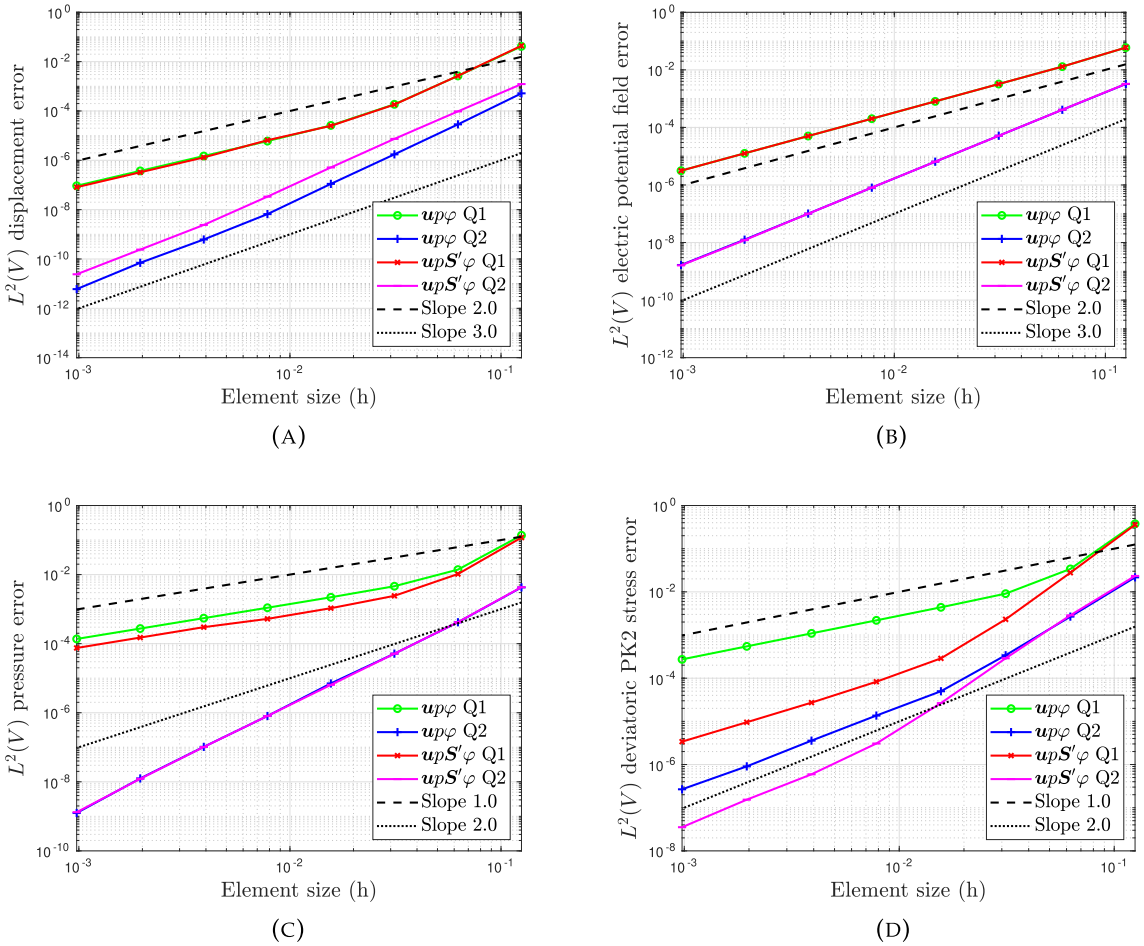

FIGURE 1 | Manufactured convergence test. Convergence rate for both $\boldsymbol{up\varphi}$ and $\boldsymbol{upS'\varphi}$ formulations upon mesh refinement. (a) Displacement error upon mesh refinement, (b) Electric potential error upon mesh refinement, (c) Pressure error upon mesh refinement, and (d) Deviatoric PK2 mechanical stress error upon mesh refinement.

The normalized error has been computed in the $L^2(V)$ norm for displacement, pressure, deviatoric PK2 mechanical stress, and electric potential fields. Figure 1a,b shows the displacement and electric potential convergence rate upon mesh size, respectively. As expected, both formulations exhibit a convergence order of $k+1$, k being the polynomial order of the FE interpolation. With respect to both pressure and deviatoric PK2 mechanical stress fields, both present the expected convergence order of k upon mesh refinement as can be observed in Figure 1c,d. The reader can note that the schemes proposed show the desired rate of convergence.

More interesting results are obtained when comparing these convergence rates with respect to DOFs in Figure 2. Figure 2a–c shows the displacement, electric potential, and pressure convergence rates upon DOFs, respectively. All fields are considered as primary unknowns of both formulations, and therefore, a similar accuracy for a given mesh size is expected, especially when linear elements are considered. Figure 2d displays the deviatoric PK2 mechanical stress convergence rates upon DOFs for both formulations. As expected, higher accuracy is achieved for a given mesh size for the mixed $\boldsymbol{upS'\varphi}$ formulation. For linear elements, to achieve the same accuracy, for example, 0.01% of global error, the $\boldsymbol{up\varphi}$ formulation requires $2.7 \cdot 10^7$ DOFs approximately, while the $\boldsymbol{upS'\varphi}$ formulation needs less than 10^5 DOFs (270 times less than the $\boldsymbol{up\varphi}$ formulation). Results clearly show that both the $\boldsymbol{upS'\varphi}$ and the $\boldsymbol{up\varphi}$ formulations deal appropriately with the incompressibility constraint, but the four-field formulation exhibits a higher accuracy in the stress field for linear elements, even for very coarse meshes.

Remark 6.1. Note that the $\boldsymbol{up\varphi}$ formulation computes the stresses (locally) at the numerical integration points, while the $\boldsymbol{upS'\varphi}$ formulation adopts a continuous stress field. To compare stress accuracy, a local smoothing technique has been applied to the original discontinuous stress fields of the mixed $\boldsymbol{up\varphi}$ formulation. So, Figures 1d and 2d present the continuous values obtained after the smoothing operation.

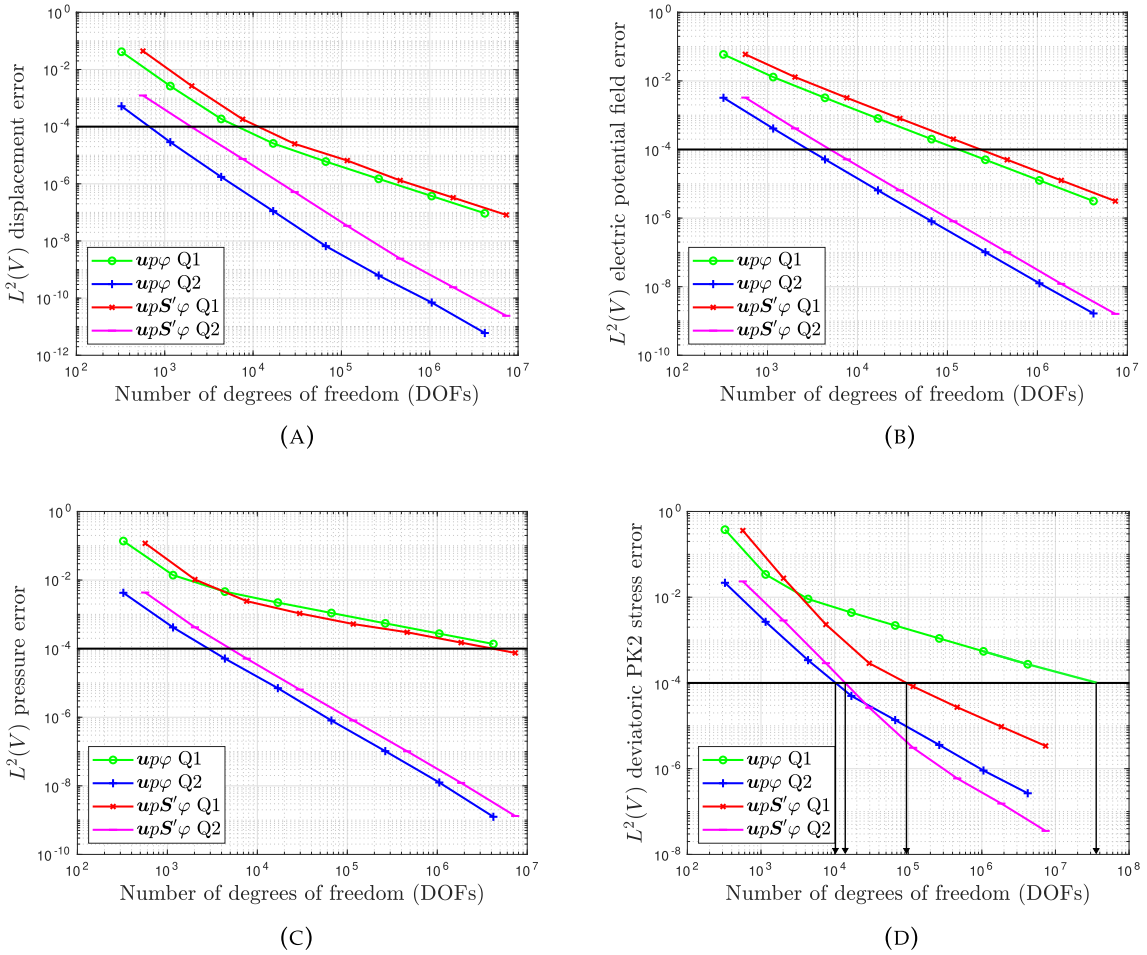

FIGURE 2 | Manufactured convergence test. Convergence rate for both $\boldsymbol{up\varphi}$ and $\boldsymbol{upS'\varphi}$ formulations upon DOFs. (a) Displacement error upon DOFs, (b) Electric potential error upon DOFs, (c) Pressure error upon DOFs, and (d) Deviatoric PK2 mechanical stress error upon DOFs.

For the sake of completeness, a study of the stabilization parameter constants has been conducted for both formulations. The objective of this study is to determine the values of the constants that yield minimal errors while maintaining the expected convergence orders and providing the minimal necessary stabilization to satisfy the inf-sup conditions of the problem. First, let us focus on the $\boldsymbol{up\varphi}$ formulation presented in Section 4.1.1. In this case, we only need to adjust the value of parameter c_1 of $\tau_{\boldsymbol{u}}$, defined in Equation (28). The results obtained for the variables of the mechanical sub-problem can be seen in Figure 3. The accuracy of the electric potential does not vary with the change in the constant.

As can be observed, the variation of the constant always maintains the expected convergence order for all variables. It is interesting to note that, in the case of Q2 elements, the precision is practically imperceptible with the variation of the parameter. On the other hand, in the case of Q1 elements, we can observe that the higher the coefficient, the greater the accuracy in displacements and the deviatoric PK2 mechanical stress, but the lower the accuracy in the pressure field. Based on the results, we conclude that c_1 should be between 0.1 and 1.0, and we will set it to 0.1 from now on. For quadratic elements, it could be taken smaller (in general, c_1 can be decreased with the polynomial order, see [78] and references therein) but, as it has already been mentioned, quadratic elements are quite insensitive to the exact value of c_1.

Regarding the $\boldsymbol{upS'\varphi}$ formulation detailed in Section 4.2.1, we now need to adjust the constants c_2 and c_3 defined in Equation (32). To do this, we first set $c_3 = 1.0$ and begin varying the value of parameter c_2. Once again, the accuracy of the electric potential is not affected. In this case, Figure 4 shows the convergence curves as a function of the variation of constant c_2. As can be observed, the conclusions regarding c_2 are exactly the same as those we previously reached for constant c_1. Therefore, we set $c_2 = c_1 = 0.1$.

Once we have fixed the constant for $\tau_{\boldsymbol{u}}$, we move on to determine the optimal value for constant c_3, related to $\tau_{\boldsymbol{S}'}$. The different convergence orders and accuracy with respect to mesh refinement can be seen in Figure 5. In this case, we observe

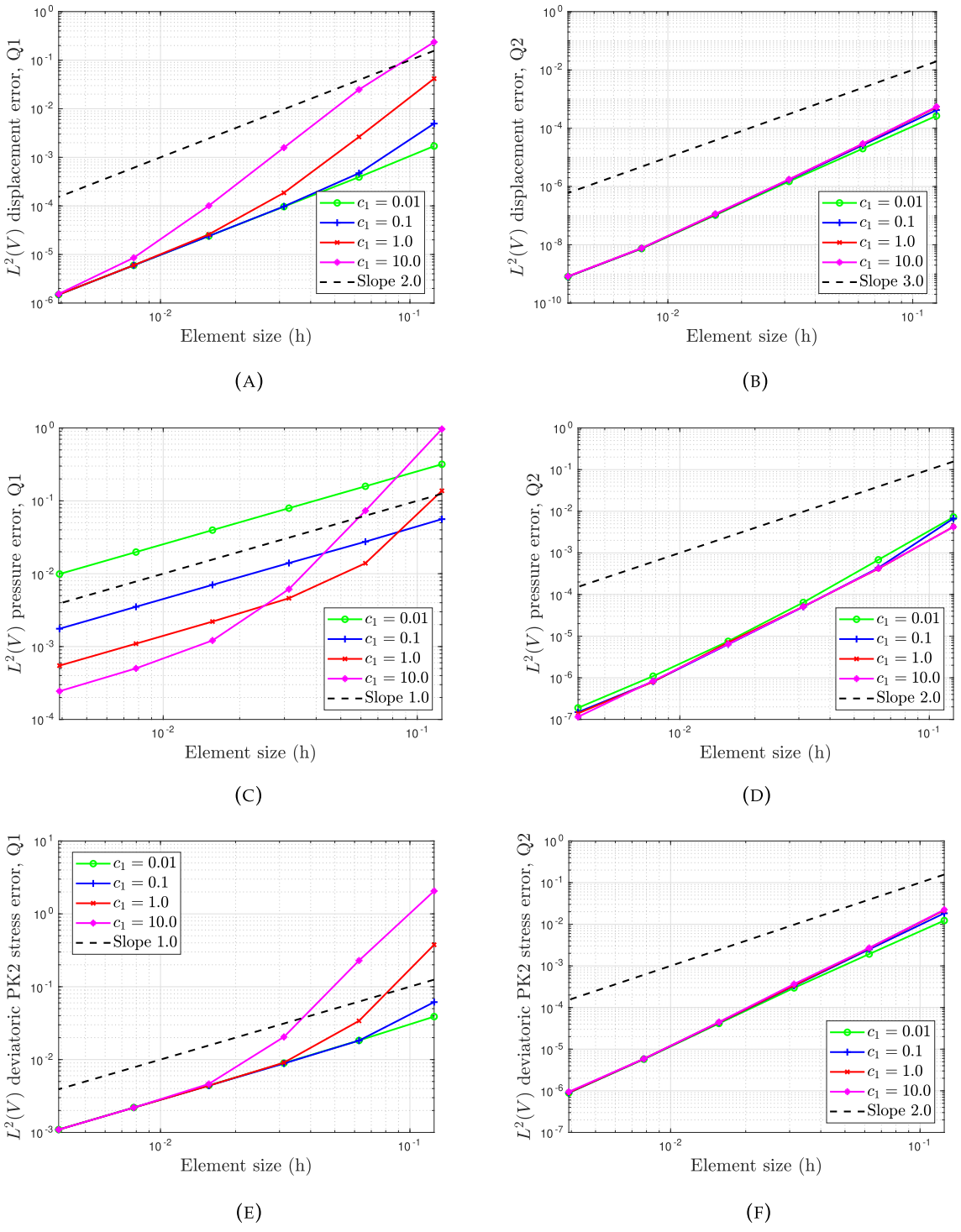

FIGURE 3 | Manufactured convergence test. Convergence rate for $\boldsymbol{up\varphi}$ formulation upon mesh refinement. Study to determine the optimal parameter c_1. (a) Displacement error upon mesh refinement, Q1 elements, (b) Displacement error upon mesh refinement, Q2 elements, (c) Pressure error upon mesh refinement, Q1 elements, (d) Pressure error upon mesh refinement, Q2 elements, (e) Deviatoric PK2 mechanical stress error upon mesh refinement, Q1 elements, and (f) Deviatoric PK2 mechanical stress error upon mesh refinement, Q2 elements.

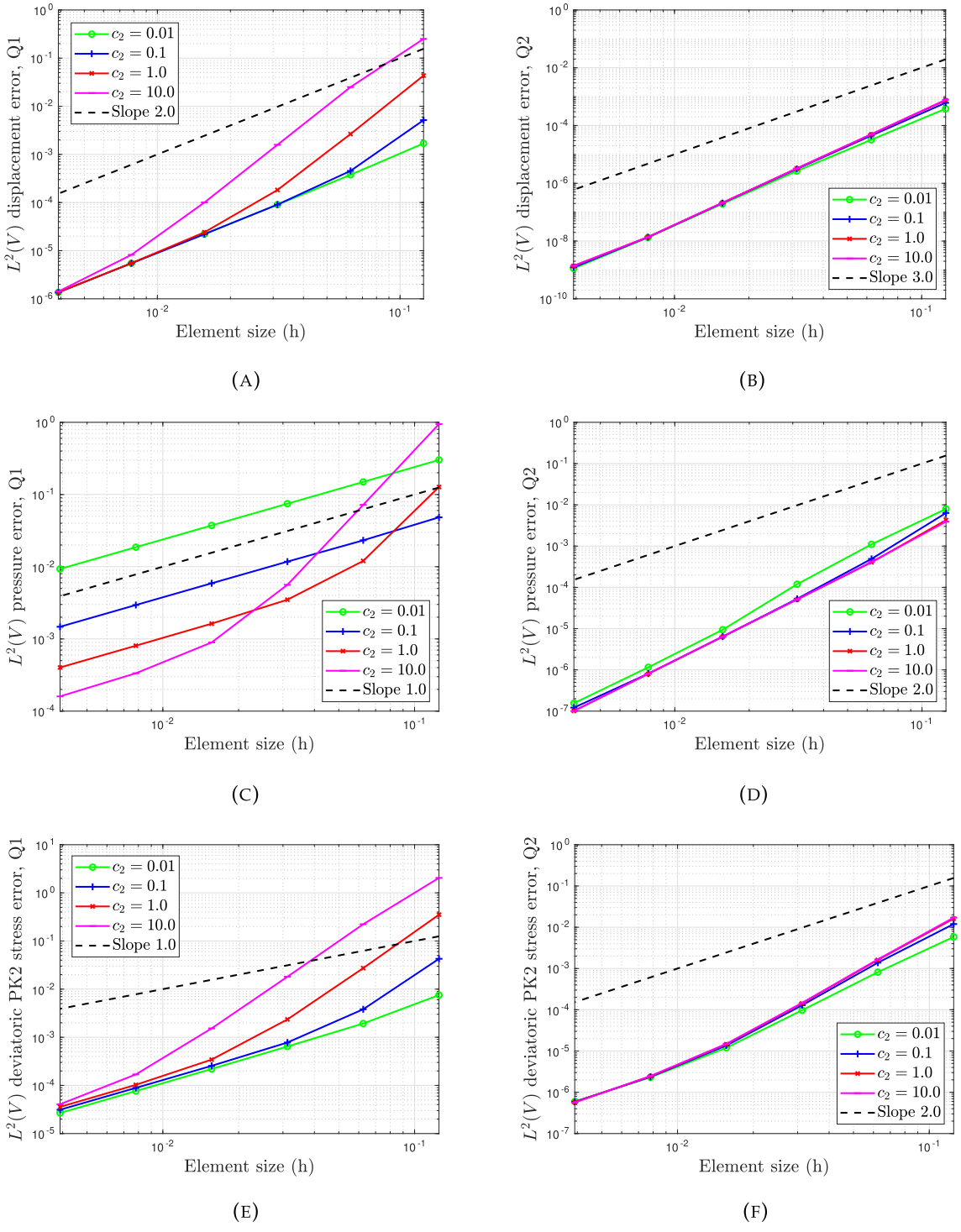

FIGURE 4 | Manufactured convergence test. Convergence rate for $\boldsymbol{upS'\varphi}$ formulation upon mesh refinement. Study to determine the optimal parameter c_2. (a) Displacement error upon mesh refinement, Q1 elements, (b) Displacement error upon mesh refinement, Q2 elements, (c) Pressure error upon mesh refinement, Q1 elements, (d) Pressure error upon mesh refinement, Q2 elements, (e) Deviatoric PK2 mechanical stress error upon mesh refinement, Q1 elements, and (f) Deviatoric PK2 mechanical stress error upon mesh refinement, Q2 elements.

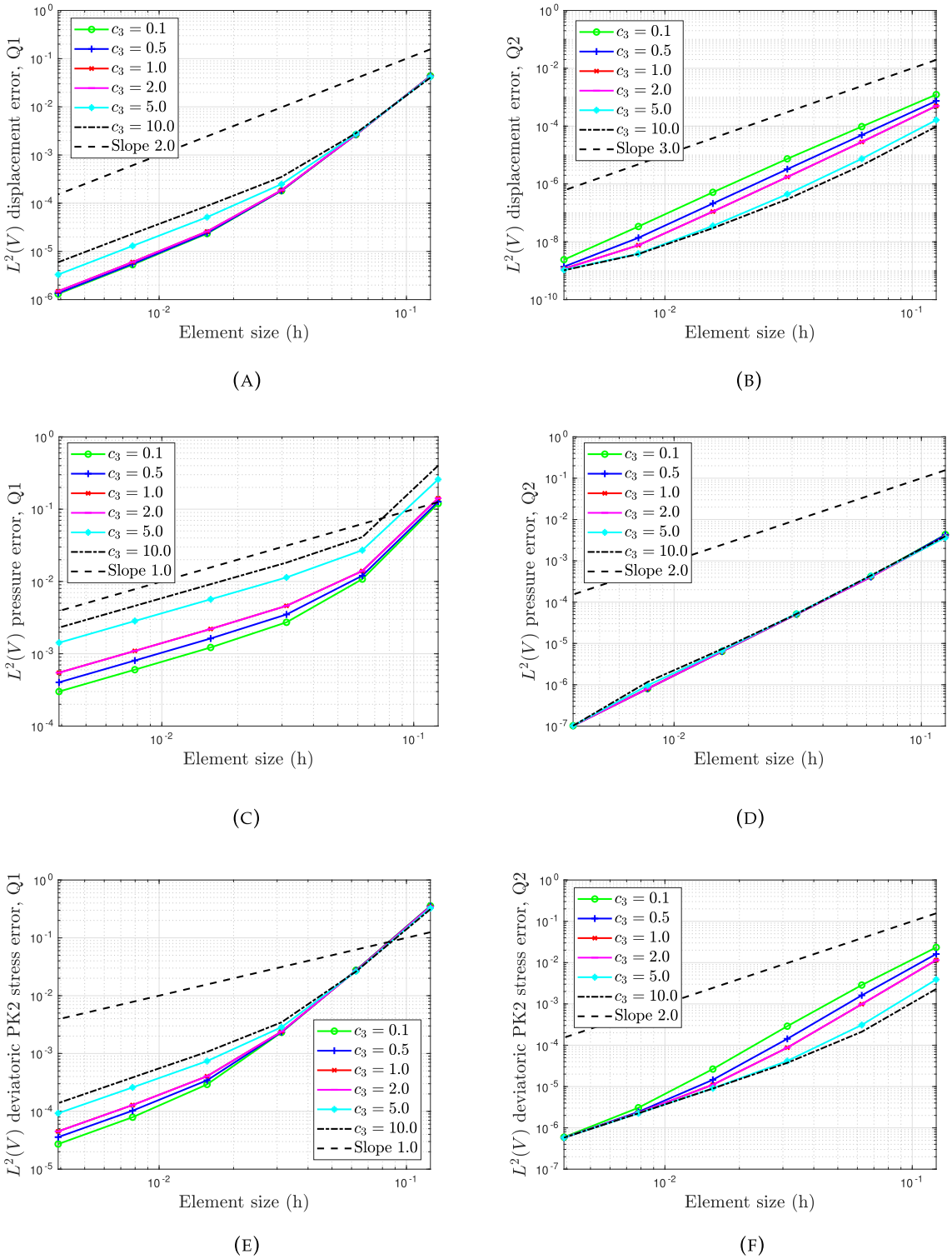

FIGURE 5 | Manufactured convergence test. Convergence rate for $\boldsymbol{upS'\varphi}$ formulation upon mesh refinement. Study to determine the optimal parameter c_3. (a) Displacement error upon mesh refinement, Q1 elements, (b) Displacement error upon mesh refinement, Q2 elements, (c) Pressure error upon mesh refinement, Q1 elements, (d) Pressure error upon mesh refinement, Q2 elements, (e) Deviatoric PK2 mechanical stress error upon mesh refinement, Q1 elements, and (f) Deviatoric PK2 mchanical stress error upon mesh refinement, Q2 elements.

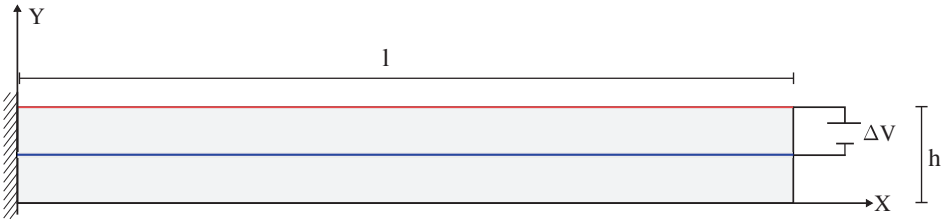

FIGURE 6 | Electrically induced bending beam. Geometry.

that for Q1 linear elements, the higher the constant, the lower the accuracy for all variables. On the other hand, when considering Q2 quadratic elements, the effect is completely reversed for displacements and deviatoric stresses, although all curves eventually tend to the same level of accuracy as we refine the mesh. However, the pressure does not appear to show any differences with the variation of the constant. For values of the constant below 0.1, the problem fails to converge, indicating that the stabilization is insufficient to guarantee the inf-sup conditions. Based on the results obtained, the optimal c_3 value should be set between 0.1 and 0.5, with 0.1 being the chosen value from this point onward. This choice still yields $c_2 = 0.1$ as an adequate value to minimize errors. For quadratic elements, the same comments as for c_1 apply now.

6.2 | Electrically Induced Bending Beam

As a second example, we will analyze the bending effect on a beam induced by a discontinuous electric field. The geometry and boundary conditions of the beam can be seen in Figure 6. The problem consists of a rectangular panel with height h and length l, clamped at the left end. Stress-free boundary conditions are applied at the remaining boundaries. The system is subject to a voltage differential ΔV to induce the bending of the beam, and electric surface charge free boundary conditions are applied on the edges. We consider a Mooney-Rivlin model (see Equation (13)) for the deviatoric component of the strain energy function with parameters $\alpha_1 = 4.83 \cdot 10^4$ Pa and $\alpha_2 = 1.74 \cdot 10^3$ Pa. For the volumetric component, a Simo-Taylor law is selected (see Equation (15)). The material is selected to be an ideal isotropic dielectric elastomer (see Equation (9)), being the electric permittivity of the dielectric $\varepsilon = 4.8\varepsilon_0$, with $\varepsilon_0 = 8.85 \cdot 10^{-12}$ F/m the vacuum permittivity.

To test the evolution of the solution while refining our mesh, the problem has been discretized into Q1 and Q2 structured meshes with N FEs along the length. Along the height, four elements are considered for all cases studied in this numerical example.

Let us study first a problem with an Aspect Ratio (AR) of 100, which means that the length of the beam is 100 times higher than the height. To do so, we fix the length of the beam to $l = 10$ cm and the height to $h = 0.1$ cm. To induce the bending of the beam, we fix the electric potential at the top side (red line) to $\varphi = 5333.37$ V and at the mid line (blue line) to $\varphi = 0$ V.

First, we aim to investigate the volumetric locking that the developed formulations may experience when dealing with nearly incompressible materials. To this end, we first consider a nearly incompressible material with a Poisson's ratio of $\nu = 0.45$, followed by an almost incompressible material with $\nu = 0.49$. The goal is to compare our mixed formulations with the irreducible formulation ($\boldsymbol{u}\varphi$-formulation) [79], where displacements and electric potential are treated as unknowns.

In Figure 7, the relative displacements obtained at the free end of the beam for the three proposed formulations can be observed. As can be seen, as the incompressibility of the material increases, the locking exhibited by the $\boldsymbol{u}\varphi$-formulation for linear elements becomes more pronounced, yielding errors of 50% in horizontal displacements and 20% in the vertical component. These errors are not observed in the mixed formulations, which allows us to confirm that they are virtually free of volumetric locking. It is also worth mentioning that this locking is corrected when quadratic elements are used, although it surely exists for values of ν closer to 0.5. In conclusion, it is important to emphasize that the irreducible formulation with linear elements is not suitable for nearly incompressible cases, as it presents a high error due to volumetric locking.

From now on, let us consider fully incompressible cases, so let us fix $\nu = 0.5$. In Figure 8, the values obtained for the relative displacement (with respect to the reference solution) can be observed for the two developed formulations using Q1 and Q2 elements. To make a fair comparison between formulations and types of elements, the evolution of displacements concerning the DOFs is studied. As can be seen, the introduction of the deviatoric PK2 mechanical stress as a primary

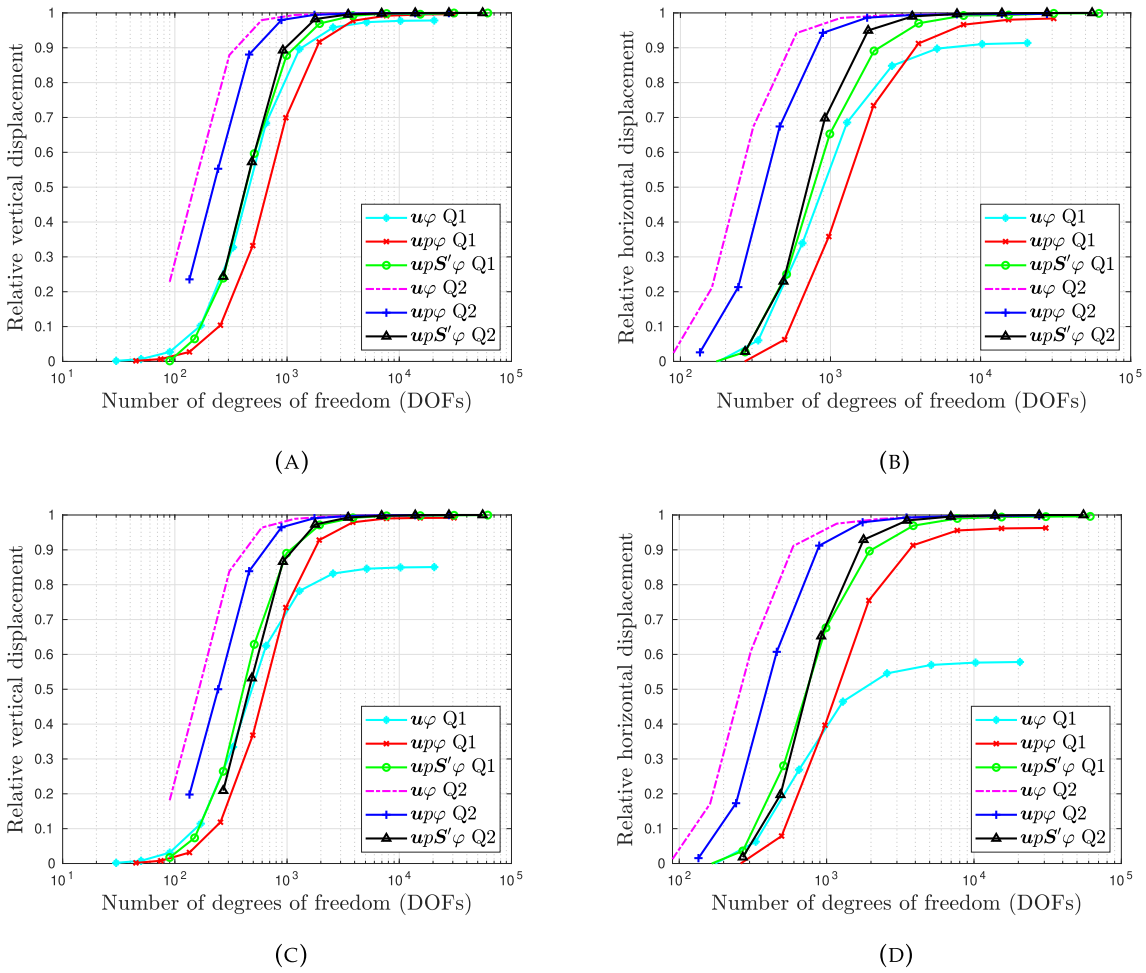

FIGURE 7 | Electrically induced bending beam. Displacement at point A for $u\varphi$, $up\varphi$ and $upS'\varphi$ formulations upon DOFs for AR = 100. (a) Relative vertical displacement upon DOFs, $\nu = 0.45$, (b) Relative horizontal displacement upon DOFs, $\nu = 0.45$, (c) Relative vertical displacement upon DOFs, $\nu = 0.49$, and (d) Relative horizontal displacement upon DOFs, $\nu = 0.49$.

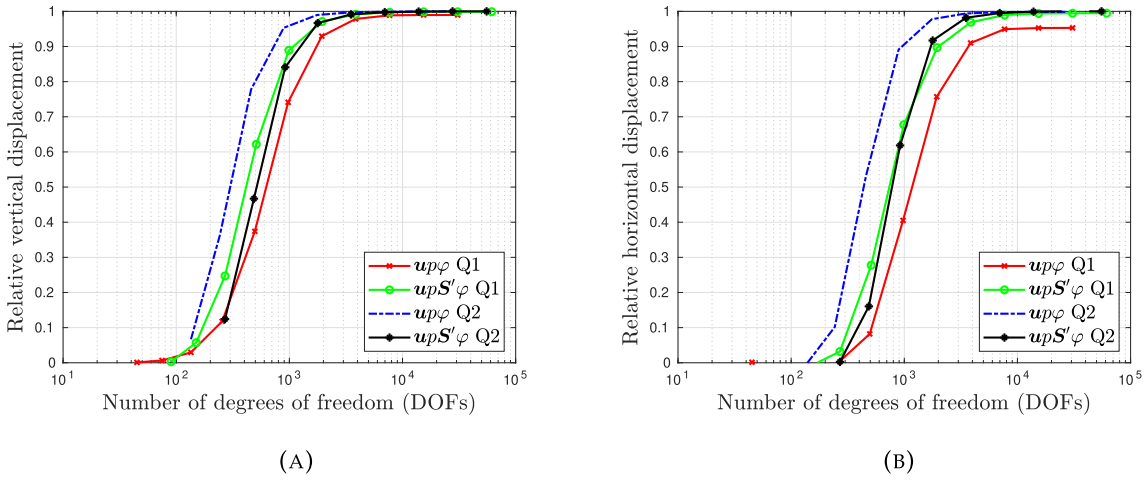

FIGURE 8 | Electrically induced bending beam. Displacement at point A for both *up* and *ups* formulations upon DOFs for AR = 100. (a) Relative vertical displacement upon DOFs, (b) Relative horizontal displacement upon DOFs.

FIGURE 9 | Electrically induced bending beam. Deformation of the beam for AR = 100, using the finest mesh with $N = 2,048$ FEs along the length. $\boldsymbol{upp}$ Q1 (red), $\boldsymbol{upp}$ Q2 (blue), $\boldsymbol{upS'p}$ Q1 (green), and $\boldsymbol{upS'p}$ Q2 (black).

variable of the problem prevents the occurrence of shear locking, which can be observed in the $\boldsymbol{upp}$ formulation. It is interesting to note that although the $\boldsymbol{upp}$ formulation with Q2 elements exhibits the fastest convergence, it should be considered that the $\boldsymbol{upS'p}$ formulation with Q2 elements will provide greater accuracy in the calculation of the deviatoric PK2 mechanical stress. Furthermore, it is worth highlighting that linear elements with the $\boldsymbol{upS'p}$ formulation are very competitive with Q2 elements for this type of problem. Figure 9 shows the final deformation obtained for both formulations with linear and quadratic elements. As previously discussed, both Q2 elements and the $\boldsymbol{upS'p}$ formulation with Q1 elements do not exhibit shear locking and converge to the same solution. In contrast, for the $\boldsymbol{upp}$ formulation with Q1 elements, shear locking is clearly observed, resulting in smaller deformations than what should actually occur (see [73, 74] for further discussion).

For the sake of exhaustiveness, we analyze the same case, but now for a much slender beam, where the length-to-height ratio is AR = 500. Thus, we fix the length of the beam to $l = 10$ cm and the height to $h = 0.02$ cm. To induce the bending of the beam, we fix the electric potential at the top side (red line) to $\varphi = 1600$ V and at the mid line (blue line) to $\varphi = 0$ V.

Figure 10 shows the relative displacement concerning the DOFs for the beam with an AR = 500. As can be observed, since the beam is now thinner, the effect of shear locking is greater in the $\boldsymbol{upp}$ formulation with Q1 elements. Again, the $\boldsymbol{upS'p}$ formulation does not exhibit this locking for Q1 elements, nor do either of the two formulations when Q2 elements are considered. This clearly demonstrates the importance of accurately capturing stresses in this type of problem, something that has already been studied and proven in cases involving plates and shields in solid mechanics [73, 74]. Finally, in Figure 11, the shear locking of the $\boldsymbol{upp}$ formulation with Q1 elements can again be observed. It is important to note that, in this case, as the beam is more slender, the locking increases, resulting in a larger discrepancy compared to the final solution presented by the other cases.

6.3 | 3D Cases

To conclude this section, two distinct cases in three dimensions will be analyzed to test the capability of our formulations under these conditions and highlight some key differences among them. This analysis will allow us to observe the performance of each formulation in a three-dimensional setting, identifying specific advantages and limitations based on the context of each case. All 3D simulations are carried out with 200 load increments to monitor the deformation of the plates as the voltage increases.

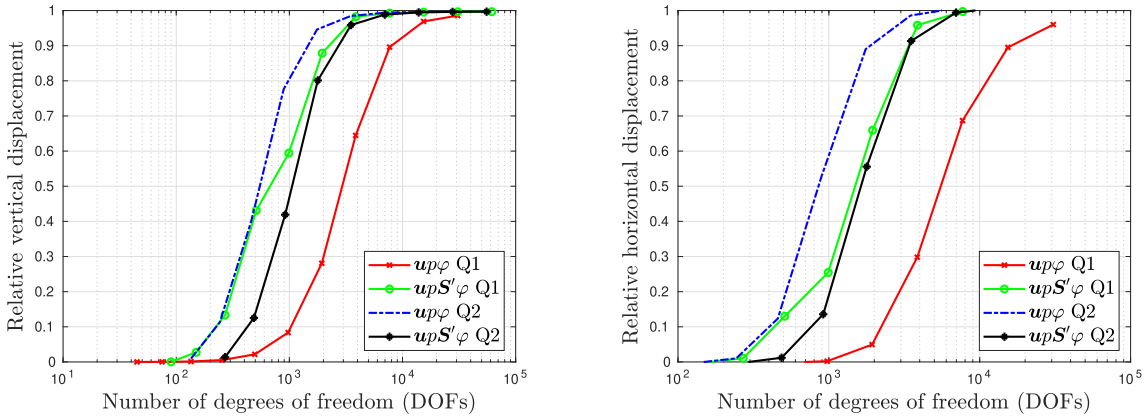

FIGURE 10 | Electrically induced bending beam. Displacement at point A for both $upφ$ and $upS'φ$ formulations upon DOFs for AR = 500. (a) Relative vertical displacement upon DOFs, (b) Relative horizontal displacement upon DOFs.

FIGURE 11 | Electrically induced bending beam. Deformation of the beam for AR = 500 using the finest mesh with $N = 2048$ FEs along the length. $upφ$ Q1 (red), $upφ$ Q2 (blue), $upS'φ$ Q1 (green), and $upS'φ$ Q2 (black).

6.3.1 | Electrically Induced Bending Plate

The objective of this numerical example is to compare the solution obtained with the different formulations developed above in scenarios where the application of an electric field on the electro-active material leads to bending-type deformations. This example considers an actuation device, as illustrated in Figure 12.

The actuation device is a parallelepiped with sides $a = 120$ mm, $b = 10$ mm, and $c = 1$ mm. The plate is fixed at the $X = 0$ end, and stress-free boundary conditions are applied to the remaining boundaries for the mechanical part. Two electrodes are placed at $Z = 0$ and $Z = c/2$ to induce bending in the plate with a voltage $\Delta V = 0.15$ mV.

Pertaining to the discretization framework, a mesh M1 with $180 \times 15 \times 4$ trilinear Q1 FEs has been judiciously employed to effectuate the interpolation of the unknowns of the problem for both formulations. To further analyze the convergence of the unknowns, a second mesh M2 with $270 \times 20 \times 4$ trilinear Q1 FEs will also be utilized.

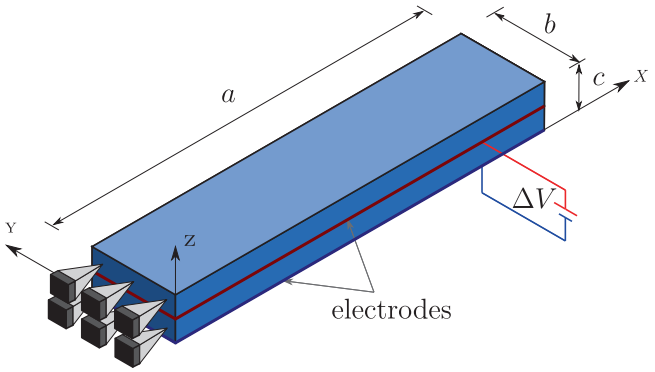

FIGURE 12 | Electrically induced bending plate. Geometry.

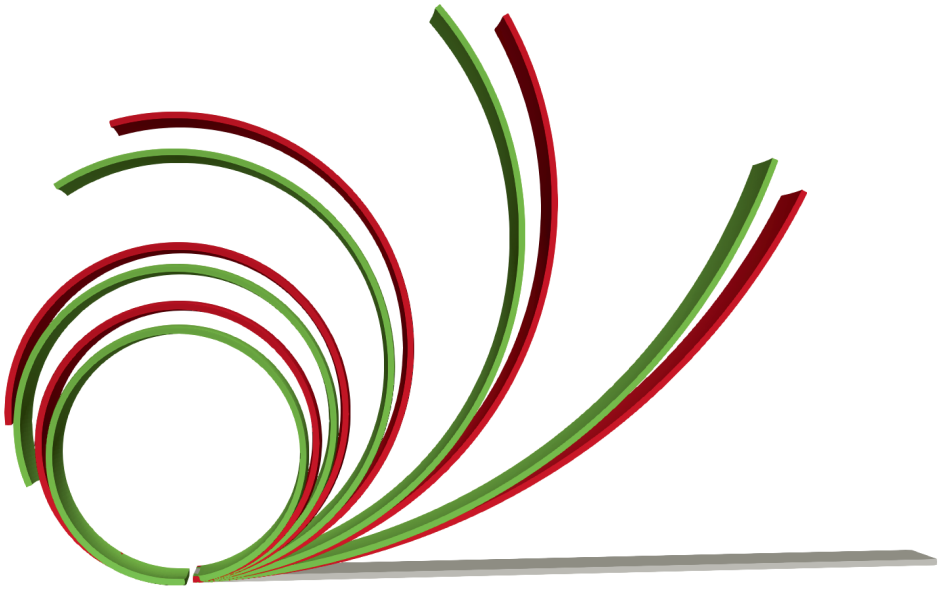

FIGURE 13 | Electrically induced bending plate. Deformation of the plate for several load increments using mesh M1. $\boldsymbol{u}p\varphi$ (red) and $\boldsymbol{u}p\boldsymbol{S}'\varphi$ (green) formulations.

In this illustrative instance, we examine a Neo-Hookean constitutive model for the deviatoric part of the strain energy, with shear modulus $\mu = 0.485$ Pa and Poisson ratio $\nu = 0.5$. A Simo-Taylor law for the volumetric model is set. The material is selected to be an ideal isotropic dielectric elastomer, being the electric permittivity of the dielectric $\varepsilon = 1$ F/m.

Figure 13 illustrates the deformations obtained for the two formulations studied at different load steps. As expected, shear locking reappears in the $\boldsymbol{u}p\varphi$ formulation when using Q1 FEs, consistent with previous findings. This issue is more pronounced due to the limitations of a linear interpolation, which fails to capture the gradients necessary for describing complex deformations. The case was also analyzed using Q2 elements, yielding the same deformations as the $\boldsymbol{u}p\boldsymbol{S}'\varphi$ formulation with Q1 elements. This highlights that the $\boldsymbol{u}p\boldsymbol{S}'\varphi$ formulation effectively mitigates shear locking, even when using linear elements.

To conclude this example, Figure 14 presents the distribution of pressure and the deviatoric component of the PK2 mechanical stress along a cross-section of the plate from point A$(1, 10, 0.5)$ to A$'(1, 0, 0.5)$ mm. This section was selected close to the clamped boundary of the plate, where high stress concentrations are expected due to the imposed constraints. The results show that the $\boldsymbol{u}p\boldsymbol{S}'\varphi$ formulation provides a more accurate representation of sharp gradients and localized peaks in the deviatoric stress field. As expected, the pressure profiles obtained with both formulations are nearly identical, since the pressure is treated as a primary unknown in both cases. This confirms that the differences in stress resolution are attributable to the introduction, as unknown, of the deviatoric stress in the $\boldsymbol{u}p\boldsymbol{S}'\varphi$ formulation.

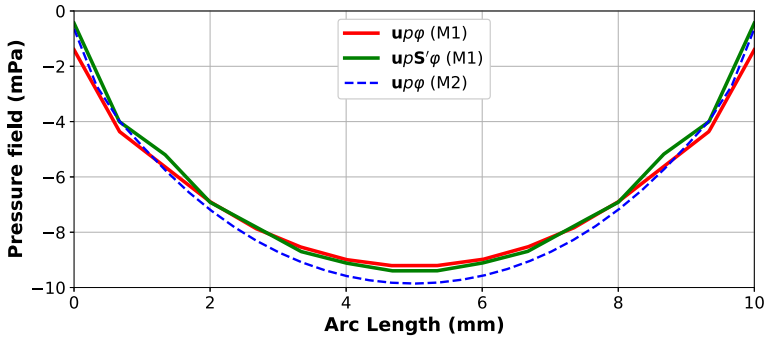

(A)

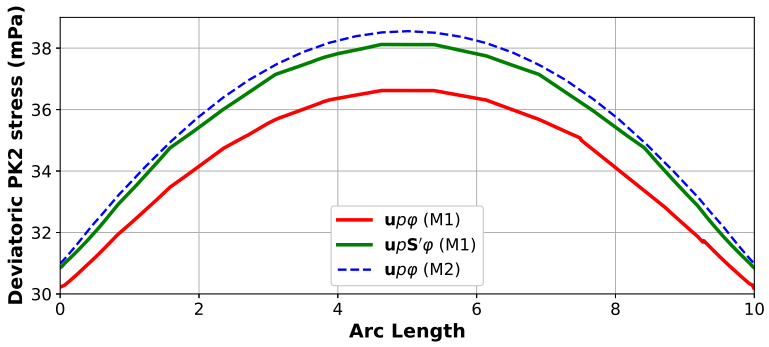

(B)

FIGURE 14 | Electrically induced bending plate. Comparison of the pressure field and the Frobenius norm of the deviatoric PK2 mechanical stress along segment A-A' for both $\boldsymbol{u}p\varphi$ and $\boldsymbol{u}p\boldsymbol{S}'\varphi$ formulations at load increment $\lambda = 0.9$. (a) Pressure field, (b) Deviatoric PK2 mechanical stress magnitude.

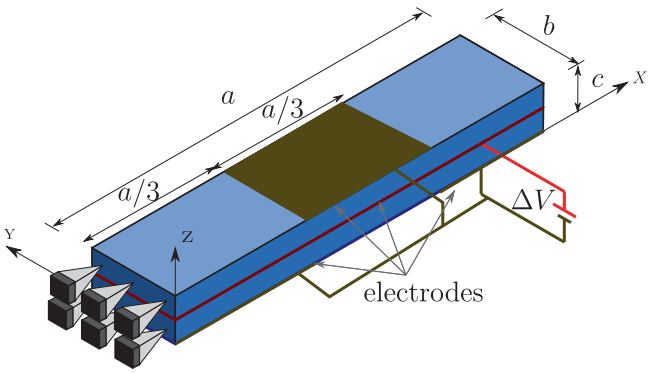

FIGURE 15 | Complex electrically induced bending plate. Geometry.

6.3.2 | Complex Electrically Induced Bending Plate

This study explores the potential of EAPs, which are often modeled as incompressible. While not all DEs are strictly incompressible, many exhibit an approximately incompressible behavior due to their high elasticity and the nature of their polymeric base. By applying localized electric potentials through strategically placed electrodes, complex deformation patterns can be induced, enabling the material to function as a dynamic actuator, sensor, or vibration dampener in response to external stimuli such as air flow, water currents, or mechanical vibrations. The example considers a cantilever beam configuration with multiple electrode pairs distributed along its surface and interior. By altering the voltage applied to these electrodes, the deformation of the beam can be finely controlled, allowing for targeted responses to external perturbations. This capability has broad implications for applications requiring adaptive control, including vibration isolation systems, flow control surfaces, and advanced sensing platforms.

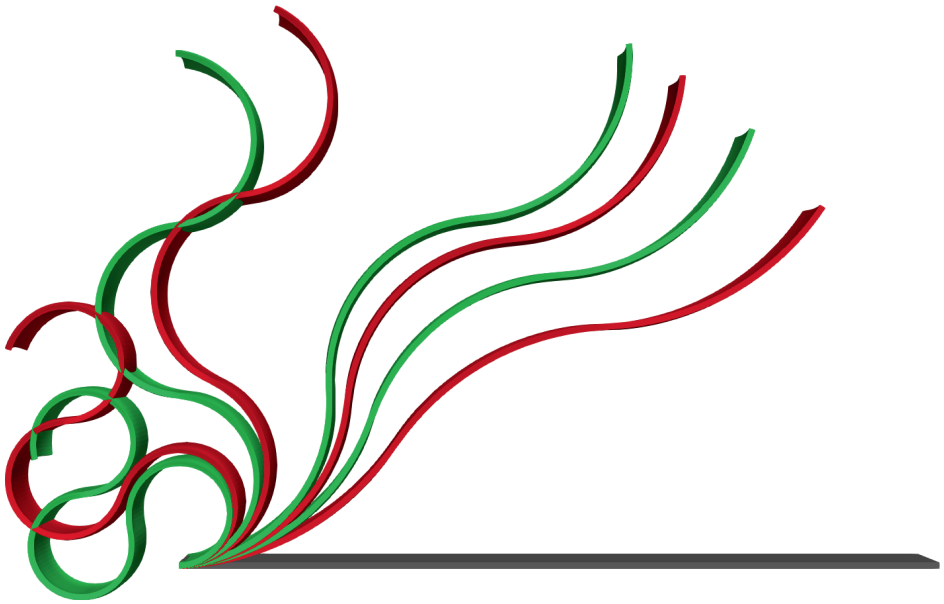

FIGURE 16 | Complex electrically induced bending plate. Deformation of the plate for several load increments. $\boldsymbol{up\varphi}$ (red) and $\boldsymbol{upS'\varphi}$ (green) formulations.

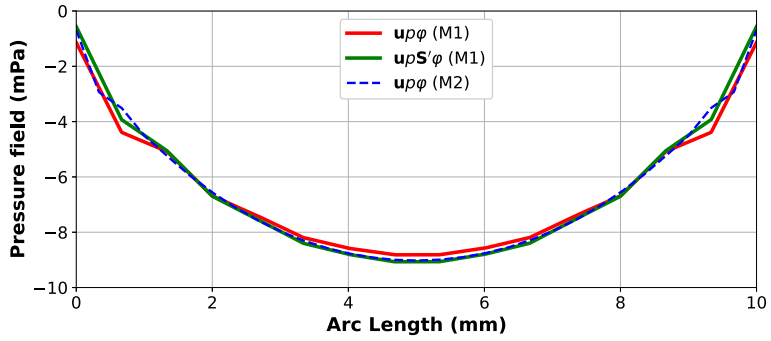

(A)

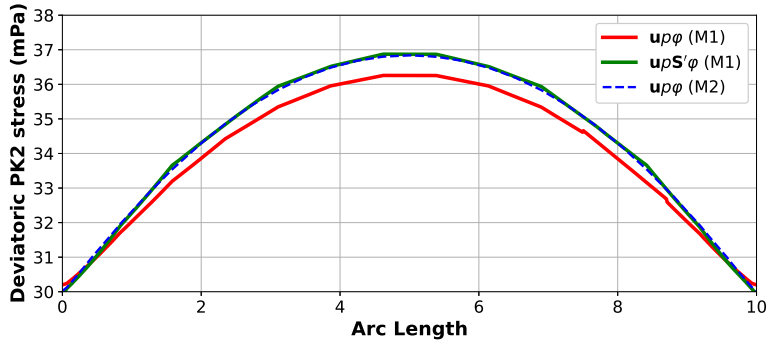

(B)

FIGURE 17 | Complex electrically induced bending plate. Comparison of the pressure field and the Frobenius norm of the deviatoric PK2 mechanical stress along segment A-A' for both $\boldsymbol{up\varphi}$ and $\boldsymbol{upS'\varphi}$ formulations at load increment $\lambda = 0.66$. (a) Pressure field, (b) Deviatoric PK2 mechanical stress magnitude.

This numerical example investigates the complex phenomenon of electrically induced bending in a cantilever beam, building upon a similar geometry and boundary conditions as in prior studies [44]. It considers the same cantilever beam as in the preceding numerical example, now subjected to a more complex set of boundary conditions for the electric potential, as illustrated in Figure 15. The same material properties, mesh discretization, and FEs as the ones taken for the previous numerical example are considered. Several electrodes are placed as it is seen in Figure 15 to reproduce a complex bending situation with a voltage $\Delta V = 0.2$ mV.

Figure 16 shows the deformations observed for the two formulations across different load steps. As expected, shear locking appears again in the $\boldsymbol{upp\varphi}$ formulation when Q1 finite elements are used, consistent with prior results. The analysis was also conducted with Q2 elements, producing deformations equivalent to those obtained with the $\boldsymbol{upS'\varphi}$ formulation using Q1 elements.

In a similar manner to Figure 14, Figure 17 presents the pressure and deviatoric PK2 mechanical stress along a cross-section of the plate for a different loading configuration. The results confirm the same trend observed previously: The $\boldsymbol{upS'\varphi}$ formulation consistently delivers a more refined capture of stress concentrations, particularly in constrained regions. This additional case reinforces the robustness and reliability of the proposed formulation across different loading scenarios.

7 | Conclusions

In this work, we have described new stabilized FE methods for the study of finite strain electromechanics when considering incompressible materials, including stress-accurate analysis.

First of all, the momentum equation is complemented with a constitutive law for the pressure which emerges from the deviatoric/volumetric decomposition of the strain energy function to formulate the mixed $\boldsymbol{upp\varphi}$ formulation presented in Section 4.1. This law is formulated properly to obtain a simple way to impose the incompressibility of the material automatically. Furthermore, to design a FE technology with a high degree of accuracy of the stress field, the constitutive law for deviatoric PK2 mechanical stresses is added to the system to obtain a monolithic system of equations for the $\boldsymbol{upS'\varphi}$ formulation stated in Section 4.2.

For both formulations, we have proposed a term-by-term (S-OSGS) type stabilization technique based on the decomposition of the unknowns into FE scales and SGSs. As it is observed in Section 6, this stabilization technique is able to circumvent the compatibility restrictions on the interpolation functions among the primary unknowns of the problem. Furthermore, the proposed schemes show the desired rate of convergence upon mesh refinement, as it can be observed in the numerical example in Section 6.1. It is interesting to note that the S-OSGS stabilization technique allows us to obtain well-defined solutions and to neglect terms that do not contribute to stability. This method turns out to be more robust for solving problems when large stress gradients are present.

Furthermore, the coupled system of algebraic nonlinear equations has been solved by means of the staggered strategy described in Section 5. This approach is advantageous for this type of coupled problem due to the saddle point issue associated with the convex/concave nature of the free energy density [30]. By solving the mechanical and electrical problems separately, the staggered approach proves to be less intrusive and more easily integrated into in-house computational platforms.

The proposed formulations are convergent upon mesh refinement, virtually free of any volumetric locking. The presented $\boldsymbol{upS'\varphi}$ technology is suitable for engineering applications in which a higher accuracy of stresses is needed. A comparison with the $\boldsymbol{upp\varphi}$ formulation is also carried out. Results clearly show that both formulations deal appropriately with the incompressibility constraint, but the three-field formulation exhibits a higher accuracy in the stress field, even for very coarse meshes.

It is important to highlight that, in many cases, dielectric elastomers exhibit a very high length-to-thickness ratio, often requiring work with very thin materials. When such materials are subjected to bending movements, it has been observed that the thinner the material, the greater the shear locking that occurs in the $\boldsymbol{upp\varphi}$ formulation with linear elements. However, when introducing deviatoric stresses as a variable, the $\boldsymbol{upS'\varphi}$ formulation does not exhibit this type of locking, making it a very appealing approach for these materials.

Acknowledgments

I. Castañar, R. Ortigosa, and J. Martínez-Frutos acknowledge the support of grant PID2022-141957OA-C22 funded by MICIU/AEI/10.13039/501100011033, Spain, and by "ERDF A way of making Europe." The authors also acknowledge the support provided by the Autonomous Community of the Region of Murcia, Spain, through the programme for the development of scientific and technical research by competitive groups (21996/PI/22), included in the Regional Program for the Promotion of Scientific and

Technical Research of Fundacion Seneca-Agencia de Ciencia Tecnologia de la Region de Murcia. R. Codina gratefully acknowledges the support received through the ICREA Acadèmia Research Program of the Catalan Government.

Conflicts of Interest

The authors declare no conflicts of interest.

Data Availability Statement

The data that support the findings of this study are available from the corresponding author upon reasonable request.

References

1. R. Pelrine, R. Kornbluh, Q. Pei, and J. Joseph, "High-Speed Electrically Actuated Elastomers With Strain Greater Than 100%," *Science* 287, no. 5454 (2000): 836–839.

2. G. Kofod, P. Sommer-Larsen, R. Kornbluh, and R. Pelrine, "Actuation Response of Polyacrylate Dielectric Elastomers," *Journal of Intelligent Material Systems and Structures* 14, no. 12 (2003): 787–793.

3. R. E. Pelrine, R. D. Kornbluh, and J. P. Joseph, "Electrostriction of Polymer Dielectrics With Compliant Electrodes as a Means of Actuation," *Sensors and Actuators A: Physical* 64, no. 1 (1998): 77–85.

4. R. Pelrine, R. D. Kornbluh, Q. Pei, et al., *Dielectric Elastomer Artificial Muscle Actuators: Toward Biomimetic Motion* (The International Society for Optics and Photonics, 2002), 126–137.

5. A. L. Skov, O. Pei, D. Opris, et al., *Dielectric Elastomers (DEs) as EAPs: Materials* (Springer International Publishing, 2016), 1–28.

6. M. Cianchetti, C. Laschi, A. Menciassi, and P. Dario, "Biomedical Applications of Soft Robotics," *Nature Reviews Materials* 3 (2018): 143.

7. S. Chiba, M. Waki, T. Wada, Y. Hirakawa, K. Masuda, and T. Ikoma, "Consistent Ocean Wave Energy Harvesting Using Electroactive Polymer (Dielectric Elastomer) Artificial Muscle Generators," *Applied Energy* 104 (2013): 497–502.

8. A. O'Halloran, F. O'Malley, and P. McHugh, "A Review on Dielectric Elastomer Actuators, Technology, Applications, and Challenges," *Journal of Applied Physics* 104, no. 7 (2008): 071101.

9. T. Li, C. Keplinger, R. Baumgartner, S. Bauer, W. Yang, and Z. Suo, "Giant Voltage-Induced Deformation in Dielectric Elastomers Near the Verge of Snap-Through Instability," *Journal of the Mechanics and Physics of Solids* 61, no. 2 (2013): 611–628.

10. X. Zhao and Z. Suo, "Electrostriction in Elastic Dielectrics Undergoing Large Deformation," *Journal of Applied Physics* 104, no. 12 (2008): 123530.

11. M. Mehnert, J. Faber, M. Hossain, S. A. Chester, and P. Steinmann, "Experimental and Numerical Investigations of the Electro-Mechanical Response of Particle Filled Elastomers — Part Ii: Continuum Modeling Approach," *European Journal of Mechanics - A/Solids* 96 (2022): 104661.

12. M. Mehnert, M. Hossain, and P. Steinmann, "A Complete Thermo–Electro–Viscoelastic Characterization of Dielectric Elastomers, Part I: Experimental Investigations," *Journal of the Mechanics and Physics of Solids* 157 (2021): 104603.

13. M. Chiumenti, M. Cervera, and R. Codina, "A Mixed Three-Field FE Formulation for Stress Accurate Analysis Including the Incompressible Limit," *Computer Methods in Applied Mechanics and Engineering* 283 (2015): 1095–1116.

14. G. Scovazzi, B. Carnes, X. Zeng, and S. Rossi, "A Simple, Stable, and Accurate Linear Tetrahedral Finite Element for Transient, Nearly, and Fully Incompressible Solid Dynamics: A Dynamic Variational Multiscale Approach," *International Journal for Numerical Methods in Engineering* 106 (2016): 799–839.

15. J. Baiges and R. Codina, "Variational Multiscale Error Estimators for Solid Mechanics Adaptive Simulations: An Orthogonal Subgrid Scale Approach," *Computer Methods in Applied Mechanics and Engineering* 325 (2017): 37–55.

16. R. Codina, I. Castañar, and J. Baiges, "Finite Element Approximation of Stabilized Mixed Models in Finite Strain Hyperelasticity Involving Displacements and Stresses and/or Pressure — An Overview of Alternatives," *International Journal for Numerical Methods in Engineering* 125, no. 18 (2024): e7540.

17. I. Castañar, J. Baiges, and R. Codina, "Topology Optimization of Incompressible Structures Subject to Fluid–Structure Interaction," *Structural and Multidisciplinary Optimization* 67, no. 90 (2024): 90.

18. D. K. Vu, P. Steinmann, and G. Possart, "Numerical Modelling of Non-Linear Electroelasticity," *International Journal for Numerical Methods in Engineering* 70, no. 6 (2007): 685–704.

19. Z. Suo, X. Zhao, and W. H. Greene, "A Nonlinear Field Theory of Deformable Dielectrics," *Journal of the Mechanics and Physics of Solids* 56, no. 2 (2008): 467–486.

20. R. M. McMeeking and C. M. Landis, "Electrostatic Forces and Stored Energy for Deformable Dielectric Materials," *Journal of Applied Mechanics* 72, no. 4 (2008): 581–590.

21. A. Dorfmann and R. W. Ogden, "Nonlinear Electroelasticity," *Acta Mechanica* 174, no. 3–4 (2005): 167–183.

22. A. Dorfmann and R. W. Ogden, "Nonlinear Electroelastic Deformations," *Journal of Elasticity* 82, no. 2 (2006): 99–127.

23. R. Bustamante, A. Dorfmann, and R. W. Ogden, "Nonlinear Electroelastostatics: A Variational Framework," *Zeitschrift für Angewandte Mathematik und Physik* 60, no. 1 (2009): 154–177.

24. S. Skatulla, C. Sansour, and A. Arockiarajan, "A Multiplicative Approach for Nonlinear Electro-Elasticity," *Computer Methods in Applied Mechanics and Engineering* 245-246 (2012): 243–255.

25. D. K. Vu and P. Steinmann, "On 3-D Coupled BEM-FEM Simulation of Nonlinear Electro-Elastostatics," *Computer Methods in Applied Mechanics and Engineering* 201-204 (2012): 82–90.

26. C. Kadapa and M. Hossain, "A Robust and Computationally Efficient Finite Element Framework for Coupled Electromechanics," *Computer Methods in Applied Mechanics and Engineering* 372 (2020): 113443.

27. R. Bustamante, A. Dorfmann, and R. W. Ogden, "On Electric Body Forces and Maxwell Stresses in Nonlinearly Electroelastic Solids," *International Journal of Engineering Science* 47, no. 11–12 (2009): 1131–1141.

28. R. Bustamante and J. Merodio, "Constitutive Structure in Coupled Non-Linear Electro-Elasticity: Invariant Descriptions and Constitutive Restrictions," *International Journal of Non-Linear Mechanics* 46, no. 10 (2011): 1315–1323.

29. R. Bustamante, "Transversely Isotropic Non-Linear Electro-Active Elastomers," *Acta Mechanica* 206, no. 3–4 (2009): 237–259.

30. A. J. Gil and R. Ortigosa, "A New Framework for Large Strain Electromechanics Based on Convex Multi-Variable Strain Energies: Variational Formulation and Material Characterisation," *Computer Methods in Applied Mechanics and Engineering* 302 (2016): 293–328.

31. R. Ortigosa and A. J. Gil, "A New Framework for Large Strain Electromechanics Based on Convex Multi-Variable Strain Energies: Finite Element Discretisation and Computational Implementation," *Computer Methods in Applied Mechanics and Engineering* 302 (2016): 329–360.

32. R. Ortigosa and A. J. Gil, "A New Framework for Large Strain Electromechanics Based on Convex Multi-Variable Strain Energies: Conservation Laws, Hyperbolicity and Extension to Electro-Magneto-Mechanics," *Computer Methods in Applied Mechanics and Engineering* 309 (2016): 202–242.

33. J. M. Ball, "Convexity Conditions and Existence Theorems in Nonlinear Elasticity," *Archive for Rational Mechanics and Analysis* 63, no. 4 (1976): 337–403.

34. J. M. Ball, *Geometry, Mechanics and Dynamics, Chapter Some Open Problems in Elasticity* (Springer, 2002), 3–59.

35. J. M. Ball and F. Murat, "$W^{1,p}$-Quasiconvexity and Variational Problems for Multiple Integrals," *Journal of Functional Analysis* 58, no. 3 (1984): 225–253.

36. P. Le Tallec, *Handbook of Numerical Analysis. Numerical Methods for Solids, Chapter 2* (North Holland, 1994).

37. P. Ciarlet, "Existence Theorems in Intrinsic Nonlinear Elasticity," *Journal Des mathématiques Pures et appliqués* 94 (2010): 229–243.

38. J. Schröder and P. Neff, "Invariant Formulation of Hyperelastic Transverse Isotropy Based on Polyconvex Free Energy Functions," *International Journal of Solids and Structures* 40 (2003): 401–445.

39. P. Neff, V. Ebbing, and J. Schröder, "Approximation of Anisotropic Elasticity Tensors at the Reference State With Polyconvex Energies," *Journal of Archive of Applied Mechanics* 79 (2009): 652–657.

40. J. Schröder, P. Neff, and V. Ebbing, "Anisotropic Polyconvex Energies on the Basis of Crystallographic Motived Structural Tensors," *Journal of the Mechanics and Physics of Solids* 56 (2008): 3486–3506.

41. M. Silhavy, "A Variational Approach to Nonlinear Electro-Magneto-Elasticity: Convexity Conditions and Existence Theorems," *Mathematics and Mechanics of Solids* 23, no. 6 (2018): 907–928.

42. F. Vogel, R. Bustamante, and P. Steinmann, "On Some Mixed Variational Principles in Electro-Elastostatics," *International Journal of Non-Linear Mechanics* 47, no. 2 (2012): 341–354.

43. M. Jabareen, "On the Modeling of Electromechanical Coupling in Electroactive Polymers Using the Mixed Finite Element Formulation," in *Procedia {IUTAM}*. Symposium on Mechanics of Soft Active Materials, vol. 12 (IUTAM, 2015), 105–115.

44. R. Ortigosa, A. J. Gil, and C. H. Lee, "A Computational Framework for Large Strain Nearly and Truly Incompressible Electromecahnics Based on Convex Multi-Variable Strain Energies," *Computer Methods in Applied Mechanics and Engineering* 310 (2016): 297–334.

45. J. Bonet, A. J. Gil, and R. Ortigosa, "A Computational Framework for Polyconvex Large Strain Elasticity," *Computer Methods in Applied Mechanics and Engineering* 283 (2015): 1061–1094.

46. J. Bonet, A. J. Gil, C. H. Lee, M. Aguirre, and R. Ortigosa, "A First Order Hyperbolic Framework for Large Strain Computational Solid Dynamics. Part I: Total Lagrangian Isothermal Elasticity," *Computer Methods in Applied Mechanics and Engineering* 283 (2015): 689–732.

47. T. J. R. Hughes, L. P. Franca, and M. Balestra, "A New Finite Element Formulation for Computational Fluid Dynamics: V. Circumventing the Babuška-Brezzi Condition: A Stable Petrov-Galerkin Formulation of the Stokes Problem Accommodating Equal-Order Interpolations," *Computer Methods in Applied Mechanics and Engineering* 59 (1986): 85–99.

48. T. Belytschko, W. K. Liu, and B. Moran, *Nonlinear Finite Elements for Continua and Structures* (Wiley, 2001).

49. T. J. R. Hughes, *The Finite Element Method: Linear Static and Dynamic Finite Element Analysis* (Prentice-Hall, 1987).

50. M. Chiumenti, Q. Valverde, C. A. de Saracibar, and M. Cervera, "A Stabilized Formulation for Incompressible Elasticity Using Linear Displacement and Pressure Interpolations," *Computer Methods in Applied Mechanics and Engineering* 191 (2002): 1095–1116.

51. R. Codina and O. Turk, "Modal Analysis of Elastic Vibrations of Incompressible Materials Using a Pressure-Stabilized Finite Element Method," *Finite Elements in Analysis and Design* 206 (2022): 103760.

52. I. Castañar, J. Baiges, R. Codina, and H. Venghauss, "Topological Derivative-Based Topology Optimization of Incompressible Structures Using Mixed Formulations," *Computer Methods in Applied Mechanics and Engineering* 390 (2022): 114438.

53. T. J. R. Hughes, G. R. Feijóo, L. Mazzei, and J. Quincy, "The Variational Multiscale Method - A Paradigm for Computational Mechanics," *Computer Methods in Applied Mechanics and Engineering* 166 (1998): 3–24.

54. R. Codina, "Finite Element Approximation of the Three Field Formulation of the Stokes Problem Using Arbitrary Interpolations," *SIAM Journal on Numerical Analysis* 47 (2009): 699–718.

55. L. Moreno, R. Codina, J. Baiges, and E. Castillo, "Logarithmic Conformation Reformulation in Viscoelastic Flow Problems Approximated by a VMS-Type Stabilized Finite Element Formulation," *Computer Methods in Applied Mechanics and Engineering* 354 (2019): 706–731.

56. L. Moreno, R. Codina, and J. Baiges, "Solution of Transient Viscoelastic Flow Problems Approximated by a Term-By-Term VMS Stabilized Finite Element Formulation Using Time-Dependent Subgrid-Scales," *Computer Methods in Applied Mechanics and Engineering* 367 (2020): 113074.

57. L. Moreno, I. Castañar, R. Codina, J. Baiges, and D. Cattoni, "Numerical Simulation of Fluid–Structure Interaction Problems With Viscoelastic Fluids Using a Log-Conformation Reformulation," *Computer Methods in Applied Mechanics and Engineering* 410 (2023): 115986.

58. I. Castañar, J. Baiges, and R. Codina, "A Stabilized Mixed Finite Element Approximation for Incompressible Finite Strain Solid Dynamics Using a Total Lagrangian Formulation," *Computer Methods in Applied Mechanics and Engineering* 368 (2020): 113164.

59. I. Castañar, R. Codina, and J. Baiges, "A Stabilized Mixed Three-Field Formulation for Stress Accurate Analysis Including the Incompressible Limit in Finite Strain Solid Dynamics," *International Journal for Numerical Methods in Engineering* 124, no. 10 (2023): 2341–2366.

60. R. Codina, "Stabilization of Incompressibility and Convection Through Orthogonal Sub-Scales in Finite Element Methods," *Computer Methods in Applied Mechanics and Engineering* 190 (2000): 1579–1599.

61. M. Cervera, R. Codina, and M. Galindo, "On the Computational Efficiency and Implementation of Block-Iterative Algorithms for Nonlinear Coupled Problems," *Engineering Computations* 13, no. 6 (1996): 4–30.

62. I. Babuška, "Error-Bounds for Finite Element Method," *Numerische Mathematik* 16, no. 4 (1971): 322–333.

63. D. Boffi, F. Brezzi, and M. Fortin, *Mixed Finite Element Methods and Applications* (Springer, 2013).

64. R. Codina, S. Badia, J. Baiges, and J. Principe, *Variational Multiscale Methods in Computational Fluid Dynamics* (John Wiley & Sons Ltd., 2017).

65. R. Codina, J. Principe, and J. Baiges, "Subscales on the Element Boundaries in the Variational Two-Scale Finite Element Method," *Computer Methods in Applied Mechanics and Engineering* 198 (2009): 838–852.

66. R. Codina, "Stabilized Finite Element Approximation of Transient Incompressible Flows Using Orthogonal Subscales," *Computer Methods in Applied Mechanics and Engineering* 191 (2002): 4295–4321.

67. J. Principe and R. Codina, "On the Stabilization Parameter in the Subgrid Scale Approximation of Scalar Convection-Diffusion-Reaction Equations on Distorted Meshes," *Computer Methods in Applied Mechanics and Enginneering* 199 (2010): 1386–1402.

68. C. O. Horgan and J. G. Murphy, "On the Volumetric Part of Strain-Energy Functions Used in the Constitutive Modeling of Slightly Compressible Solid Rubbers," *International Journal of Solids and Structures* 46 (2009): 3028–3085.

69. J. C. Simo, R. L. Taylor, and K. S. Pister, "Variational and Projection Methods for the Volume Constraint in Finite Deformation Elasto-Plasticity," *Computer Methods in Applied Mechanics and Engineering* 51, no. 1–3 (1985): 177–208.

70. J. Bonet and R. D. Wood, *Nonlinear Continuum Mechanics for Finite Element Analysis* (Cambridge University Press, 1997).

71. J. Schröder, P. Neff, and D. Balzani, "A Variational Approach for Materially Stable Anisotropic Hyperelasticity," *International Journal of Solids and Structures* 42 (2005): 4352–4371.

72. J. M. Ball, "Energy-Minimising Configurations in Nonlinear Elasticity," *Archive for Rational Mechanics and Analysis* 63, no. 4 (1976): 337–403.

73. A. Aguirre, R. Codina, and J. Baiges, "Stress–Displacement Stabilized Finite Element Analysis of Thin Structures Using Solid-Shell Elements, Part I: On the Need of Interpolating the Stresses," *Finite Elements in Analysis and Design* 236 (2024): 104168.

74. A. Aguirre, R. Codina, J. Baiges, and I. Castañar, "Stress–Displacement Stabilized Finite Element Analysis of Thin Structures Using Solid-Shell Elements, Part II: Finite Strain Hyperelasticity," *Finite Elements in Analysis and Design* 236 (2024): 104179.

75. J. Martínez-Frutos, R. Ortigosa, and A. J. Gil, "In-Silico Design of Electrode Meso-Architecture for Shape Morphing Dielectric Elastomers," *Journal of the Mechanics and Physics of Solids* 157 (2021): 104594.

76. S. Balay, S. Abhyankar, M. F. Adams, et al., "PETSc Web Page," (2015), http://www.mcs.anl.gov/petsc.

77. D. N. Arnold, R. S. Falk, and R. Winther, "Mixed ?Nite Element Methods for Linear Elasticity With Weakly Imposed Symmetry," *Mathematics of Computation* 76 (2007): 1699–1723.

78. R. Codina, "On *hp* Convergence of Stabilized Finite Element Approximations of the Convection-Diffusion Equation," *SeMA Journal* 75 (2018): 591–606.

79. R. Poya, A. J. Gil, R. Ortigosa, R. Sevilla, J. Bonet, and W. A. Wall, "A Curvilinear High Order Finite Element Framework for Electromechanics: From Linearised Electro-Elasticity to Massively Deformable Dielectric Elastomers," *Computer Methods in Applied Mechanics and Engineering* 329 (2018): 75–117.